Assessing the destructiveness of tropical cyclone by anthropogenic aerosols under an atmosphere-ocean coupled framework

Yun Lin[1,2], Yuan Wang[3,*], Jen-Shan Hsieh[1], Jonathan H. Jiang[4], Qiong Su[5,6], Lijun Zhao[1], Michael Lavallee[1], Renyi Zhang[1,*]

[1]Department of Atmospheric Sciences, Texas A&M University, College Station, Texas 77843, USA.

[2]Joint Institute for Regional Earth System Science and Engineering, University of California, Los Angeles, California 90095, USA.

[3]Department of Earth System Science, Stanford University, Stanford, California 94305, USA.

[4]Jet propulsion Laboratory, California Institute of Technology, Pasadena, California 91109, USA.

[5]Department of Water Management & Hydrological Science, Texas A&M University, College Station, TX, USA

[6]Department of Agricultural Sciences, Clemson University, Clemson, SC, USA,

Corresponding authors: Yuan Wang (yzwang@stanford.edu) and Renyi Zhang (renyi-zhang@geos.tamu.edu)

Abstract

Intense tropical cyclones (TCs) can cause catastrophic damages to coastal regions after landfall. Recent studies have linked the TC's devastation to climate change that induces favorable conditions, such as increasing sea-surface temperature, to supercharge the storms. Meanwhile, environmental factors, such as atmospheric aerosols, also impact the development and intensity of TCs, but their effects remain poorly understood, particularly coupled with the ocean dynamics. Here we quantitatively assess the aerosol microphysical effects and aerosol-modified ocean feedbacks during Hurricane Katrina using a cloud-resolving atmosphere-ocean coupled model - Weather Research and Forecasting (WRF) in conjunction with the Regional Ocean Model System (ROMS). Our model simulations reveal that an enhanced destructive power of the storm, as reflected by larger integrated kinetic energy, heavier precipitation, and higher sea-level rise, is linked to the combined effects of aerosols and ocean feedbacks. These effects further result in an expansion of the storm circulation with a reduced intensity because of decreasing moist static energy supply and enhancing vorticity Rossby wave outward propagation. Both accumulated precipitation and storm surge are enhanced during the mature stage with elevated aerosol concentrations, implying exacerbated flooding damage over the coastal region. The ocean feedback following the aerosol microphysical effects tends to mitigate the vertical mixing cooling in the ocean mixing layer and offsets the aerosol-induced storm weakening, by enhancing cloud and precipitation near the eyewall region. Our results highlight the importance of accounting for the effects of aerosol microphysics and ocean-coupling feedbacks to improve the forecast of TC destructiveness, particularly near the heavily polluted coastal regions along the Gulf of Mexico.

1. Introduction

The destruction of Hurricane Katrina that struck New Orleans, Louisiana in late August 2005 was measured by the maximum wind speed at landfall and the hundreds of kilometers of the coast areas affected by severe storm surge of more than 3 m. Hurricane Katrina progressed inland as a category 3 storm (with sustained winds of 194 km hour^{-1}) and generated significant storm surge exceeding 10 m on the Mississippi coast and up to 6 m southeast of New Orleans, with up to 2 m of additional wave run-up in the most exposed location (Fritz et al., 2007; NWS, 2016). The catastrophic damage associated with hurricanes in recent decades is exemplified as the evidence of increasing devastation of tropical cyclones (TCs) relevant to changing climate (Emanuel, 2005, 2017; Knutson et al., 2019; van Oldenborgh et al., 2017), which induces favorable environmental conditions (such as increasing SST) to supercharge hurricanes and increase the risk of major damage (Trenberth et al., 2018). Another key feature of TC lies in the efficient formation of hydrometeors and large latent heat release that fuels the TC development and destruction via strong winds, heavy precipitation, storm surge, and flooding (Pan et al., 2020). Currently, the effects of the abovementioned factors on the destructive power of TCs remain to be quantified and isolated.

There now exist compelling evidence that natural and anthropogenic aerosols play critical roles in the genesis and development of TCs from both observational and modeling perspectives (Khain et al., 2010; Herbener et al., 2014; Khain et al., 2016; Pan et al., 2018; Sun and Zhao et al., 2020; Rosenfeld et al., 2012; Wang et al., 2014). By acting as cloud condensation nuclei (CCN), aerosol particles can lower the requirement of supersaturated condition for cloud formation (Fan et al., 2018; Wang et al., 2011). A previous modeling study demonstrated that high aerosol levels invigorate rainbands and increase precipitation, but decrease the eyewall strength (Zhang et al., 2009; Khain et al., 2010; Rosenfeld et al., 2012; Wang et al., 2014). Particularly for Hurricane Katrina, Khain et al. (2008; 2010) and Wang et al. (2014) found that aerosols can enhance cloud formation at the hurricane periphery via enhancing the convection over there, suppress the convection over the eyewall and therefore weaken the hurricane intensity. Another recent observational analysis also corroborated that anthropogenic aerosols enlarge the rainfall area of TCs over the northwestern Pacific (Zhao et al., 2018). However, the aerosol microphysical effects are not represented in most operational forecast models, such as the Hurricane - Weather Research and Forecasting (HWRF), since the number concentrations of CCN/cloud droplets are prescribed in the microphysics schemes in simulating cloud formation and development in TCs (Zhang et al., 2018). Additionally, the pristine maritime level of the CCN/cloud droplets prescribed in those models (Zhang et al., 2018) greatly underrepresented the aerosol condition over land (Zhang et al., 2015). In addition to being a major metropolitan area for New Orleans, the coastal areas along the Gulf of Mexico host many industrial facilities, i.e., power plants, chemical manufactories, and petroleum refineries with large industrial emissions of anthropogenic aerosols (Fan et al., 2005; Fan et al., 2006; Levy et al., 2013), which have been shown to considerably influence convection, lightning, and precipitation (Orville et al., 2001; Fan et al., 2007a, b; Li et al., 2009). More recently, Souri et al. (2020) reported the aerosols over Houston tend to cause a moderate increase in precipitation, but the reference simulation was not comprehensively evaluated by observations.

Air-sea interaction represents another crucial determinant factor of TC storm intensity and structure (Black et al., 2007; Emanuel, 1986; Green and Zhang, 2014; Liu et al., 1979). One such typical air-sea interaction is sea surface cooling due to vertical mixing, sometimes due to the Ekman upwelling when storms move slowly, as TCs pass by the ocean, which can lead to negative feedback to storm intensity because the cooler deep ocean temperature underneath the TC storm suppresses heat and moisture transfer from the ocean surface to the storm circulation and eventually weakens storm (Bender et al., 1993; Khain and Ginis, 1991; Ma et al., 2013; Schade & Emanuel, 1999). In addition to modulating storm intensity, the change of SST can also alter storm size and precipitation features (Chavas et al., 2016; Lin et al., 2015). As such, an inclusion of air-sea interaction into models could have profound impacts on TC simulations (Bender and Ginis, 2000).

Most of previous modeling studies adopted either fixed or prescribed SST from reanalysis data to drive TC simulations (e.g., Zhang et al., 2009; Rosenfeld et al., 2011; Wang et al., 2014), likely leading to significant biases in evaluating aerosol effects on TC storms due to the absence of ocean feedbacks. Recently, Lynn et al. (2016) and Khain et al. (2016) found that both aerosols and ocean coupling show significant effects on Hurricane Irene development, particularly on the timing of hurricane's intensity evolution; but their use of 1-D ocean model coupled with WRF appears underestimates the SST cooling produced by the hurricane by about 1℃ relative to observation. One plausible reason is that the 1-D ocean model may be unable to accurately represent three-dimension physical processes in the ocean mixing layer, such as convergence and its associated upwelling as TC passes (Yablonsky and Ginis, 2009). Therefore, a 3-D ocean model coupled with the atmosphere model is a more advanced tool to obtain more accurate vertical mixing and/or upwelling cooling and thereby more accurate aerosol effect on TC power.

Missing of air-sea interaction introduces biases into TC simulations, and there is still lack of studies on the aerosol effect on TC with ocean coupling. Therefore, it is necessary to improve the understanding of how ocean coupling interacts with TC evolutions under external forcing, and if the ocean coupling plays a role, to what extent it can modify the aerosol effect on TC development. Therefore, the primary purpose of this study is to evaluate the ocean feedbacks following aerosol microphysical effects, particularly from storm's damage perspective, including precipitation and storm surge. To address these questions, we need an advanced modeling tool to accurately capture air-sea interactions, particularly the SST response in simulations. In this regard, we employ a 3-D atmosphere-ocean coupled cloud-resolving model, i.e., the advanced WRF version 3.6 (Skamarock and Klemp, 2008) coupled with the Regional Ocean Modeling System (Patricola et al., 2012) to simulate the evolution of Hurricane Katrina (2005) with a full consideration of air-sea interactions. The aerosol microphysical effect on the TC destructiveness is explicitly evaluated using an aerosol-aware two-moment bulk microphysical scheme (Li et al., 2008). Moreover, we evaluate the role of ocean coupling in the aerosol-hurricane system and the aerosol-induced ocean feedback by comparing coupled simulations with delicately designed uncoupled simulations. Hurricane Katrina is selected as the case for this modeling study is because it can well serve our research goals aiming to evaluate the combined effects of aerosol and ocean coupling feedback on the destructiveness of a typical tropical cyclone due to 1) its most severe storm surge on record in U.S. and 2) the like role of ocean coupling feedback in modulating the destructiveness power of the storm.

2. Model and Experiments

The aerosol-aware two-moment bulk microphysical scheme, developed at Texas A&M University (hereafter referred to as the TAMU scheme), is implemented into WRF to represent thirty-two microphysical processes and aerosol-cloud interactions (Li et al., 2008). The TAMU scheme has been employed to evaluate the aerosol microphysical effect on various systems, including mesoscale convective system (Wang et al., 2011), squall line (Li et al., 2009), TC (Wang et al., 2014), and continental cloud complex (Lin et al., 2016; Wang et al., 2018). The scheme contains five hydrometeor categories, i.e., cloud droplet, rain drop, ice crystal, snow, and graupel.

The cloud droplet number concentration is prognostically predicted through the formation from the aerosol activation based on the Köhler theory and the water vapor supersaturation computed by WRF. More detailed descriptions of TAMU scheme can be found in Li et al. (2008). The effect of ice nuclei particles is not considered in the microphysical scheme used in our model.

Both WRF and ROMS are configured on the same Arakawa C grid at 3-km resolution yet with 50 and 35 vertical levels, respectively. The horizontal grid spacing of 3 km fulfills the minimum requirement to represent the dynamical and microphysical responses of hurricanes to aerosols (Rosenfeld et al., 2012). The WRF simulation domain covers the entire Mexico Gulf and the southern portion of the United States (75° W – 100° W; 17° N – 38° N) and a slightly smaller domain is configured for ROMS (Fig. 1a). The atmospheric initial and boundary conditions for WRF are set up by interpolating the data of the 6-hourly NCEP Climate Forecast System Reanalysis (CFSR, Saha et al., 2010) to the 3-km WRF grid for the simulation period from August 27 to August 31 2005. The initial and boundary conditions for ROMS simulations of the same period of time are specified using the Hybrid Coordinate Ocean Model (HYCOM, https://hycom.org/) Gulf of Mexico Reanalysis dataset with a horizontal resolution of 1/25°. The same dataset is used to provide the SST over the oceanic regions outside of the ROMS domain.

We carry out three primary experiments to examine the combined effects of aerosols and air-sea coupling and to compare their relative importance in an aerosol-hurricane-ocean coupled system. Based on the Moderate Resolution Imaging Spectroradiometer (MODIS) aerosol optical depth (AOD) measurements, averaged over the periods prior to and during Hurricane Katrina passage in 2005 over the Gulf of Mexico (Aug. 24 – Aug. 31), it was found that there is a clear land-ocean contrast in aerosol spatial distribution (Fig. 1a), i.e., the concentration over land is two folds of that over ocean for all the simulations. As such, the horizontal distribution of the initial aerosol number concentration in simulations mimics the land-ocean contrast as observed in AOD distribution. Over land and ocean, the aerosol concentration was uniformly distributed. The initial and boundary aerosol concentration setups for both clean and polluted conditions are following Wang et al. (2014). The three experiments in this study are listed in Table 1: (1) the coupled experiment with the initial and boundary aerosol concentration of 200 cm^{-3} (100 cm^{-3}) over land (ocean) at the surface level, representing typical clean maritime environment (hereafter C_C case); (2) the coupled experiment with the aerosol's initial and boundary concentrations of 1000 cm^{-3} (500 cm^{-3}) over land (ocean) (hereafter P_C case), as shown in Fig. 1b; and (3) the uncoupled experiment with prescribed SST obtained from the C_C case and aerosol settings the same as the P_C case (hereafter P_UC case), which is together with P_C case to isolate the aerosol-induced ocean feedbacks on TC development. As such, the initial aerosol concentrations in all polluted simulations are five times higher than that in all clean cases. With similar model configuration, Wang et al. (2014) reported that the five times of aerosol concentration contrast between clean and polluted conditions show clear aerosol effect signature in tropical cyclone development. In order to evaluate the impacts of ocean coupling itself on TC responses to aerosol loadings, we perform an additional pair of non-coupling simulations, namely C_UC_HYCOM and P_UC_HYCOM, in which the SST is fixed and constrained by the HYCOM dataset and with the exactly same aerosol settings as the pair of coupled simulations, i.e., C_C and P_C (Table 1). To mimic the emissions from the continent, aerosols can be continuously advected from the lateral boundaries (Khain et al., 2010). An exponential decreasing profile is assumed for the initial aerosol vertical distribution, following Wang et al. (2014) and similar as Khain et al. (2016).

Ammonium sulphate ($(NH4)_2SO_4$) is assumed as the chemical component of polluted continental aerosols. In addition, given that sea salt is an important source of giant CCN in the central zone of the storm (Rosenfeld et al., 2012), in this study we parameterize the emissions of sea salt (NaCl) as a function of surface wind speed, following Binkowski and Roselle (2003) and Zhang (2005). The initial concentration of sea salt is set equal to 100 cm^{-3} for all simulations, consistent with Khain et al. (2016) and Lynn et al. (2016). As the hurricane develops, more sea salt particles are generated by surface wind turbulence at the vicinity of the storm eyewall than the outside regions, since the strengthening wind near the hurricane eyewall leads to more sea salt spray. Recent studies suggest that sea salt particles may play appreciable role in altering tropical cyclones (Shpund et al., 2019; Shi et al., 2021). For instance, Shpund et al. (2019) reveals that these sea salt particles can give rise of additional droplets in the eyewall and may lead to a positive feedback in which TC intensifies with the increase in the maximum wind. However, this effect is not taken into account in this study yet as our focus is on the effect of polluted continental aerosols. The simulated AOD in pollluted case is about 0.55 at the domain boundaries and about 0.20 averaged over the inner domain, comparable to the MODIS measurements in the Gulf of Mexico and the nearby coastal regions. Also, the observed aerosol mass concentration over the Gulf of Mexico region is reported about 7 g m^{-3} from the field measurements (Bate et al., 2008; Levy et al., 2013), consistent with the polluted cases in this study. In addition, during hurricane development, e.g., at around 18:00 UTC, 27 August 2005 when MODIS mearurements are available (not shown), it is found that the simulation and the MODIS retrieval show similarity in spatial and clear aerosol bands from the continent intruding into the storm system over the ocean.

To properly isolate each individual effect of aerosols and ocean feedback from their combined effect, we examine the aerosol effect on TCs with and without proper ocean feedback by comparing the coupled simulations (C_C and P_C cases) with an uncoupled one prescribed with the SST obtained from our coupled C_C case. The combined effects of aerosol and ocean coupling can be manifested by the differences between P_C and C_C. The independent effect of the aerosol can be estimated by contrasting P_UC and C_C given that the SST is identical in these two cases. The aerosol-modified ocean feedback, i.e., the modified ocean response to TCs when the aerosol effect is present, can be assessed by the differences between the results of the P_C and P_UC cases. Besides the aerosol-induced ocean responses, we are also interested in how and to what extent the ocean coupling can modify the aerosol effect on TC storm. In this regard, we perform comparison of the differences between the changes of the non-coupling simulations (i.e., P_UC_HYCOM - C_UC_HYCOM) and the changes of the coupled simulations (i.e., P_UC_HYCOM - C_UC_HYCOM).

3. Results

3.1 Vertical mixing cooling and storm intensity

The WRF-ROMS model used in this study in general performs well in modeling Hurricane Katrina when comparing against observations. For example, the simulated storm track of the hurricane shows a good agreement with the best track from NHC, particularly on 28-29 August, 2005 (Fig. S1a). The radius of maximum wind (RMW) of the polluted storms on 29 August, 2005 falls in the observed range between 45-55 km (Fig. S1b; NHC, 2023). The simulations generally reproduce the typical features of Katrina evolution in terms of minimal sea-level pressure (SLP) and maximum surface wind speed (Figs. 2a and b), but the peak time is somehow delayed in both coupled or uncoupled polluted cases.

The model also well captures the spatial shape of the cold band observed after Katrina passed the Gulf of Mexico, as evident in the good match of the simulated SST cooling with the remote sensing observations (Fig. S2). Also, it shows better performance than the reanalysis data of HYCOM (Figs. S2e and h). Since the hurricane track of the polluted coupled case (P_C) generally follows that of the clean coupled case (C_C), the aerosol-modified ocean feedback in vertical mixing cooling can be approximately estimated by subtracting the simulated SST of the C_C case from that of the P_C case. Fig. S2k displays the overall SST cooling difference between the P_C case and the C_C case just before Katrina's landfall in New Orleans. The spatial pattern of the SST difference following the passages of the two simulated hurricanes demonstrates a slightly lagged ocean response, which shows that aerosols cause the changes in hurricane that further induce less vertical mixing cooling (positive SST difference) near the storm inner core but more cooling away from the storm center. The vertical mixing coolings become discernible after 10 hours of the WRF-ROMS coupled simulations in both experiments with different aerosol concentrations (Figs. 3a and b). During the period of 10-30 hour, the azimuthally mean SST difference between the P_C case and the C_C case shows weak positive and negative patches changing irregularly with time (Fig. 3c). Such an irregular pattern of the SST difference mainly results from the slightly southward shift (about 20-30 km) of a more wobbling hurricane track in the P_C case compared to the C_C case (Fig. S1a). In addition, the negative SST anomalies between 10–30 hour are likely due to the track shift (blue and red solid curves in Fig. S2k) and the different storm translation speeds between the two cases (blue and red solid lines in Fig. 3c). The storm translation affects SST since vertical mixing and upwelling of cold deep ocean water would be more sustained when the storm moves more slowly and thereby the cooling can be stronger. As the storm moves forward, the SST responses induced by aerosols become more significant during 30-55 hour, with notable less cooling over the region close to the storm inner core (< 50 km from the storm center) while more cooling over the region where the storm periphery locates (100 km away from the storm center).

As for the storm intensity, the uncoupled clean case with prescribed HYCOM SST (i.e., C_UC_HYCOM) simulates the strongest storm, and then the storm intensity is greatly reduced under polluted condition even without ocean coupling (i.e., P_UC_HYCOM), which is associated with the aerosol weakening effect similar as proposed previously (Khain et al. 2008; Khain et al. 2010; Rosenfeld et al., 2012; Wang et al., 2014). The advanced atmosphere-ocean coupled modeling framework enables us to assess the ocean coupling effect and its feedback caused by the aerosol effect on TC. Figs. 3a and b show that the simulated storm intensity can be further significantly reduced by the ocean coupling effect under both clean and polluted conditions. To quantify the ocean coupling impact on the aerosol weakening effect, we derive the differences in minimal SLP and maximal surface wind speed between the clean and polluted simulations for the both uncoupled and coupled simulations pairs (Figs. 3c and d). It is found that the differences in minimal SLP and maximal surface wind speed for the coupled and uncoupled simulation pairs are similar before about 50 hours, indicating that the ocean coupling effect does not exert marked impacts on the storm intensity change caused by the aerosol effect at the storm developing and mature stages. As the storm starts to dissipate after 48 hours but before 60 hours, the difference in minimal SLP (maximal surface wind speed) for the coupled simulation pair is larger (more negative) than the uncoupled one. In other words, the ocean coupling effect at the storm dissipating stage (48-60 hours) can sustain a longer and more significant aerosol weakening effect than the case without ocean coupling. In fact, the aerosol effect for the uncoupled simulations diminishes quickly as TC dissipates as the difference caused by the aerosol effect decreases to zero with a relatively large rate (Fig. 3c).

The differences between the two polluted cases with and without ocean coupling (P_C and P_UC) denote the ocean coupling feedbacks following aerosol microphysical effects since both cases contain the aerosol weakening effect associated with the similar loading of aerosol pollution. Before the storm reaches its peak the minimal SLP and maximal surface wind speed of P_UC are slightly larger than P_C and this trend is reversed during the short period just after the storm peak. However, the relatively small differences in minimal SLP and maximal surface wind speed between P_UC and P_C indicate that the aerosol-modified ocean coupling feedbacks does not play a major role in modulating TC's peak intensity/strength.

3.2 Precipitation

The simulated TC exhibits distinct structures in terms of rainbands under the three aerosol and ocean coupling scenarios (Fig. 4). The TC simulated in the two polluted cases (i.e., P_UC and P_C) exhibits invigorated rainbands at the developing state (24 h), and these effects become more evident when the TC approaches toward the land under higher aerosol concentrations as shown in Fig. 4 at 46 h and 52 h. The invigorated rainbands in the two polluted cases are associated with a weakened storm intensity and delayed storm intensification, as shown in the lower (higher) peak (nadir) maximum surface wind speed (minimum sea level pressure), and the slower increase (decrease) in maximum surface wind speed (minimum sea level pressure) in Figs. 3a and b. The intensification of the rainbands under the polluted condition also accelerates the formation of the double-eyewall structure, which is about 6 h earlier (at around 46 h) than in the C_C case (at 52 h, Fig. 5a). The inner eyewall in the two polluted cases eventually dissipates at the landfall (60 h) since most of the moisture and angular momentum are used to sustain the outer eyewall, resulting in a singular larger eye. Overall, the two polluted cases exhibit noticeably enlarged storm size and enhanced precipitation rate near the eyewall when the storms approach the land, consistent with previous studies (e.g., Khain et al. 2010, Rosenfeld et al. 2012, Wang et al. 2014, etc.).

Although the aerosol-modified ocean coupling feedbacks is minor factor affecting TC's peak intensity/strength, it significantly changes the precipitation distribution, leading to a more contracted rainband and further enhanced precipitation rate near the eyewall, e.g., an annulus heavy rain belt locates at around 60-80 km away from the TC center at the landfall (60 h) under P_C case (Fig. 4c).

The TC storm with possible enhanced storm surge and precipitation rate near the TC landfall can both significantly increase the disastrous threat of coastal flooding, which is the most damaging aspect of TC impacts in coastal regions (Woodruff et al., 2013). A further examination of the temporal and spatial evolution of the precipitation rate reveals that the aerosol-modified ocean coupling effect can significantly change precipitation distribution and enhance precipitation rate within 100 km of the TC center when TC approaches toward the land (45-60 h, Figs. 5a and c). Both two polluted cases exhibit increased azimuthally-averaged profiles precipitation rate primarily at 60-100 km away from the TC center, especially under the P_C case (Fig. 5d). Flooding is largely determined by accumulated precipitation within certain areas and time. To assess the flooding severity, we calculate the total accumulated precipitation within 100 km of the TC center, particularly during the period of the TC approaching toward the land. As shown in Fig. 5e, the total precipitation during the mature stage of TC on average increases by 22% in P_C case and 11% in P_UC relative to C_C, indicating a higher flooding potential under elevated aerosol conditions, especially with the consideration of ocean coupling.

3.3 Storm surge

To further assess the aerosol impact on storm surge and strong wind damage, the storm destructiveness potential is calculated by taking both TC intensity and TC influenced marine wind fields into account. The integrated kinetic energy (IKE_{TS}) index is used here as a proxy for the hurricane destructive potential (Emanuel, 2005). It is the summation of the squares of all grid cell with marine winds greater than the tropical storm force wind (i.e., 18 m s^{-1}) multiplying the volume with a vertical depth of 1 m centered at the 10 m-level layer. While high aerosol concentrations weaken the intensity of the storm (assessed by point values like max wind or min SLP), our simulations reveal an enhanced destructive power of the storm together with an increased storm surge under elevated aerosol conditions (Figs. 6 and 7). As shown in Fig. 6a, the polluted cases release more destructive energy than the clean one, particularly at the Katrina's landfall (at 60 h). For example, the P_C case releases 11 TJ more kinetic energy than the C_C case. On average, the IKE_{TS} for P_C is 18% higher than C_C over the entire hurricane lifecycle. The enhanced storm destructiveness is attributed to the expansion of the storm circulation (Figs. 6b) to produce higher surface winds beyond the eyewall region and a larger area of tropical storm force (Fig. 8a). With the ocean coupling, the IKE_{TS} for P_C slightly decreases by less than 5% relative to P_UC as the storm approaches to land. From Fig. 8b it is also found that the wind outside of the eyewall is stronger in P_UC than P_C from hour 50 to 60, which is responsible for the higher destructiveness in P_UC at this time period. This also suggests that ocean coupling plays a minor role in modulating the damages corresponding to strong wind and storm surge.

As a direct indicator of storm surge, the sea level height is simulated with the integration of the 3-D ocean model ROMS (Fig. 7). Our simulation generally captures the peak timing and magnitude of observed sea level height at Dauphin Island, AL (Fig. 7a). Albeit the insufficient gauge measurement at other stations, the simulated peak sea level heights are comparable to the recorded values at New Canal and Shell Beach stations (Fritz et al., 2008). The polluted TC can produce a more than 50 cm higher storm surge than the clean one (Figs. 7 and 9a), suggesting that the TC likely causes more severe damage by storm surge along the coastal area under polluted condition than clean condition. Given that storm surge associated with tropical cyclones can be determined by both the strength and orientation of winds relative to coastline, we derive and examine three snapshots of the wind speed difference between the coupled polluted and clean simulations (Fig. 9b) as well as wind vectors for the two cases (Fig. 9c) over New Orleans coastal area when Katrina passed over. The alternating high and low sea-level height anomalies can be interpreted by the combined effects of the changes in wind intensity and orientation when storm approaches the coastal regions. For instance, the stronger surface wind (i.e., positive difference in wind speed) cyclonically around the storm are found at certain shore regions, e.g., near Shell Beach at 64 hours and Dauphin Island at 65 hours. The enhanced wind can push more water toward the shore, and more water can pile up over the shore, eventually leading to more severe storm surge under the polluted condition. As for the significant negative anomalies in sea-level height from clean to polluted aerosol conditions, e.g., at 65 hours over the Mississippi-Alabama coast to the west of the Dauphin Island site (Fig. 9a), it is found that there are the less perpendicular wind vectors to the coastline in the P_C case than that in the C_C case, resulting in less efficient water pileup in the P_C case when the wind push water to the shore.

3.4 Storm structure redistribution

The modifications on precipitation characteristics and storm destructiveness by aerosols are mainly due to storm intensity changes and structural redistribution under the high aerosol scenarios. The underlying physical mechanism can be further revealed by examining the vertical-radial cross-sections of the dynamic and thermodynamic of the storm (Fig. 10). By serving as CCNs, the elevated aerosols tend to suppress warm rain process and invigorate mixed- and ice-phase clouds in outer rainbands and significantly change latent heat distribution. As shown in Fig. 10a, P_C case exhibits higher ice water content (IWC) in outer rainbands and a more divergent latent heating distribution with reduced latent heating near the eyewall and enhanced latent heating over the area 40-100 km away from the storm center.

The enhanced heat flux outward the eyewall is associated with the enhanced propagation of vortex Rossby waves (VRWs) which accelerate the tangential winds near the RMW of the polluted storm (Figs. S3 and 4). The VRWs theories have been widely used to explain the storm intensity and structural changes, as well as the formation of spiral rainband in TC (Houze et al., 2007; Montgomery and Kallenbach, 1997; Wang, 2002). The enhanced outward propagation of VRWs under polluted cases transport more angular momentum from the eyewall to the outer rainbands, accelerating tangential wind in the rainbands at the cost of decelerating the tangential wind in the eyewall (Figs. S3 and 4). A further examination of the corresponding potential vorticity (PV) field shows that aerosol can significantly change the vortex structure by weakening its overall vorticity (Fig. 10b) and subsequently reduce the β drift of the hurricane. To conserve angular momentum during the vorticity rearrangement, some of the high eyewall vorticity is also fluxed outward, taking on the form of outward-propagating VRWs. These waves rotate cyclonically with the high PV core and propagate radially outward and stagnate at radii of 70–90 km, where the radial potential vorticity gradient disappears or reverses its sign. In the polluted case, the large gradient of equivalent potential temperature (θ_e) between 6-9 km suggests a more stable condition, which favors the VRWs propagation outward along radial direction (Fig. 10c). Moreover, the evaporative cooling of rainbands can result in significant downdrafts, which often bring cool and dry air (i.e., smaller moist static energy supply) into the inflow boundary layer. For example, the relative lower θ_e is observed at outer rainbands (>45 km) at 0-3 km high of the atmosphere under the polluted case than the clean case by up to 3 K. The air flow with this lower moist static energy might be transported and mixed into the eyewall, further contributing the weakening of the eyewall convection and thus the reduction of the storm intensity.

Since the storm development is highly influenced by the energy gained from ocean water, it is necessary to examine the dynamic and thermodynamic processes occurring at the air-sea interface to further elucidate the mechanisms leading to the storm structural modifications by the aerosol and ocean coupling effects. To first examine the aerosol effect on the TC evolution without ocean feedback, we compare the pollutant uncoupled case (P_UC) with those of the clean coupled case (C_C), both of which are forced with the same SST distribution in the model. Fig. 11a shows the differences of the total surface heat flux and wind stress magnitudes between P_UC and C_C. Of the most prominent feature is the significant surface heat flux deficiency (surplus) well correlated with negative (positive) wind stress difference within about 25-50 km distance from the storm center throughout most periods of the whole simulation, except some very brief periods of time. This suggests that surface heat flux near the core region (approximately within RMS) is mainly driven by the magnitude of surface wind stress rather than moisture flux difference. On the other hand, over 50 km away from the center, the surface heat flux and wind stress differences in the pollutant uncoupled case are all generally larger than those of the clean coupled case. The significant negative surface heat flux difference around 50 to 100 km distance from the center is associated with the higher surface heat flux in the clean coupled case, which arises due to the drier descending air in the moat area of the double eyewall forming between hours 57 and 60.

Here we evaluate the impact of SST difference induced by the aerosol-contaminated TC on the surface heat flux and wind stress distributions, which manifests the contributions of ocean feedback to the pollutant TC aloft. Fig. 11b displays the surface heat flux and wind stress differences between the pollutant coupled (P_C) and uncoupled (P_UC) cases. In general, we expect to see a relatively higher SST in the wake of the TC in the pollutant cases than that in the clean case due to a weaker vertical mixing response to a pollutant TC. However, due to the discrepancy of some slight track deviation between the pollutant case and the clean coupled case, some relatively lower near-center SST can also be experienced by the pollutant TC core compared to the clean TC core, which thus contribute to the formation of negative surface heat flux and wind stress differences, as displayed in the Hovemuller diagram. This is the case for the significant surface heat flux deficit overlapping with surface wind stress deficit between hour 12 and 42, which is associated with a slightly leftward deviation of the TC track in P_UC as compared with that of P_C (see Fig. S1a), leading to the pollutant TC of the uncoupled case surrounded by relatively cooler SST. After the TCs turn more northwards approaching the warm Loop Current Eddy around 90.5 W and 27 N, the tracks of both TCs nearly always overlap with each other until landfall, where more symmetrically positive (negative) SST difference near (off) the TC cores can be observed (see Fig. S2 and Fig. 11b). The colocations of both the positive and negative surface heat flux and wind stress differences after hour 42 well manifest a clear air-sea coupling signal: the warmer (cooler) SST not only causes more (less) surface heat flux but also increase (decrease) the magnitude of surface wind stress by enhancing (reducing) the turbulent momentum mixing downwards from the free atmosphere to ocean surface. This further indicates that a strong vertical mixing and Ekman upwelling tends to decouple the near-surface flow from the flow on the top of boundary layer, reducing the dynamic and thermodynamic forcing of the TC to the ocean beneath.

Fig. 11c shows the combined effect of aerosols and air-sea interaction on the surface heat flux and wind stress distributions of the TC. The surface heat flux and wind stress differences show some characteristics similar to those in Fig. 11a yet they demonstrate a better correlation with each other than the pollutant case without proper ocean feedback, especially during the time from hour

42 to 60 before landfall. Note that the evident surface heat flux deficit before hour 60 is well correlated with the wind stress deficit under the combined effect of aerosols and air-sea coupling, in contrast to the result shown in Fig. 11a, in which negative surface heat flux difference is collocated with positive surface wind stress difference. Of particular interest is that the seemingly quasi-periodic burstings of high surface heat flux difference due to the aerosol effect (Fig. 11a) turn into sporadic bursts of heat flux and wind stress anomalies in Fig. 11c, suggesting that a proper air-sea coupling, as reflected by the strength of ocean feedback modulated by an aerosol-contaminated TC, still plays a role in affecting the magnitudes of surface heat flux and wind stress of a pollutant TC and thus its precipitation distribution moving with the TC.

To be more clearly quantitatively view the dynamic and thermodynamic processes occurring at the air-sea interface response to aerosol and ocean coupling, we derive azimuthally-averaged radial profiles at the ocean surface for the three aerosol and ocean coupling scenarios averaged over two periods, i.e., the typical period of storm developing stage (15-28 hours) and the typical period of storm mature stage (42-55 hours, Fig. 12). On average the lower surface heat flux in P_C than P_UC at the developing stage (left column in Figs. 12a and b) is due to the relatively cooler near-center SST, which is caused by the slight deviation of the TC track in the two polluted cases in comparison with the clean case (Fig. S1). Without consideration of the track shift in P_C relative to C_C case, the vertical mixing cooling strength in C_C case is actually very close to P_C at this stage (Fig. 12b), suggesting that the change of ocean feedback strength due to the aerosol effect on the TC is still not strong enough at the beginning stage to significantly impact the TC aloft. This can be evidence in the relatively small differences in surface wind stress and total water path formed in the storm among the three cases (Figs. 12c and d). This is further confirmed by little changes in precipitation (Fig. 5) or storm destructiveness (Fig. 6) of P_C from P_UC cases at the developing stage. However, as the TC approaches toward the land with higher aerosols concentrations, the ocean feedback starts to affect the evolution of the TC. At the mature stage (42-55 hr), the SST feedback shows a warm core with a time average of azimuthally mean SST up to 0.5℃ warmer in P_C than that in C_C and a slightly colder periphery. The SST warming (cooling) near the inner core (the periphery) increases (reduces) the thermal energy transfer to the storm eyewall (outer rainbands). Thus, a weaker vertical mixing cooling near the center of the polluted TC reciprocally increases the coupling between the near-surface flow and the aloft free atmosphere flow, providing relatively more surface heat flux near the eyewall of the polluted TC, as positive feedback to sustain the strength of the TC aloft. Consequently, the aerosol-modified ocean feedback significantly enhances the cloud formation and precipitation rate near the eyewall (Figs. 12d and 5d). The enhanced cloud formation in turn results in larger latent heat release aloft over the region just outside of 50 km away from the storm center (Fig. S5), which further strengthens the cloud convection and may also contribute to the enhancement of cloud formation in the storm. Also note that the peak winds shift farther from the center, suggesting that the eye of the polluted hurricane gets larger, which is evident in Fig. S1b as well.

4. Summary and conclusions

In this study, we quantitatively assess the aerosol microphysical effect and aerosol-induced ocean feedback on the development and destructiveness of a tropical cyclone (TC). For the first time, a three-dimension atmosphere-ocean fully coupled regional model (WRF-ROMS) at the cloud-resolving scale was used to simulate Hurricane Katrina to investigate the aerosol-TC system with inclusion of air-sea interaction.

Our atmosphere-ocean coupled modeling framework clearly detects significant ocean response in SST induced by the aerosol effect as the storm approaches to its mature stage (e.g., after 30 hours of the WRF-ROMS simulation). Moreover, our study reveals that anthropogenic aerosols enlarge the air circulation of the storm as well as the rainbands with weakened storm intensity and delayed storm intensification. The comparison of the aerosol weakening effect between the simulations with and without ocean coupling suggests that ocean coupling can sustain more significant aerosol effect at the storm dissipating stage. With an increase in aerosol concentration by five times, the total precipitation within 100 km of the TC center during the mature stage increases by 22% and 11% with and without ocean coupling, respectively, suggesting a high flooding-potential under elevated aerosol conditions, especially with the consideration of air-sea interaction. The integrated kinetic energy, which is an indicator of storm surge and strong wind damage, increases by 18% from the clean to polluted aerosol conditions over the entire hurricane lifecycle. The ocean feedback due to the aerosol effect (i.e., aerosol-modified ocean coupling effect) on the TC intensity is minimal at the beginning stage but plays a significant role in precipitation distribution, especially as the TC approaches landfall with higher aerosols concentrations.

Our work elucidates the underlying mechanisms through which aerosols and ocean coupling affect the storm structure and intensity as well as the destructive power, as depicted in Fig. 13. When approaching landfall aerosols can invigorate the mixed- and ice-phase clouds in TC periphery by serving as CCN with additional latent heat release aloft at the rainbands, enhancing outward propagation of vortex Rossby waves from the eyewall regions. The aerosol effect also induces a lower equivalent potential temperature in the inflow within the boundary layer because of evaporative cooling of rainbands, leading to reduced moist static energy transited to the storm center. More significant outward propagation of VRWs and less moist static energy supply leads to weakening of the storm eyewall but enlarged storm circulation. With inclusion of the ocean coupling effect, the vertical mixing cooling near the eyewall reciprocally increases the interaction between the near-surface flow and the aloft free atmosphere flow, thus providing larger surface heat flux near the eyewall to sustain the strength of the TC aloft. Overall, the combined aerosol effects result in a noticeably enhanced precipitation rate and strengthened storm destructiveness with enhanced storm surge and enlarged circulation, both significantly contributing to coastal flooding.

Our study demonstrates that accurate prediction of TC development and destructiveness requires the representation of atmosphere-ocean coupling in hurricane forecast models, because of the significant vertical mixing cooling and its considerable feedbacks to the storm. Our results show that aerosols play a prominent role in modulating the TC storm intensity and structure with the inclusion of ocean coupling effect, corroborating the notion that the aerosol effects cannot be neglected in the TC forecast models. Despite a case study conducted, the identified mechanisms and modeling technique of this study are generalizable for the study of aerosol-tropical cyclone interactions. Specifically, the application of the 3D cloud-resolving, aerosol-aware atmosphere-ocean coupled modeling technique (i.e., WRF-ROMS) in this study paves the way for its utilization in investigating other case studies involving interactions between aerosols and tropical cyclones. Notably, our study showcases the superior performance of the WRF-ROMS model compared to a 1-D ocean model coupled with WRF in accurately simulating vertical mixing and upwelling cooling under TC storms. Moreover, while acknowledging the case-specific nature of these relationships, it is conceivable that the elucidated physical mechanisms hold varying degrees of significance across diverse hurricane systems, contingent upon aerosol pollution conditions and thermodynamic contexts. Hence the direct generalizability may vary, but the insights gleaned from our study can serve as a valuable reference point for future inquiries that seek to unravel the complexities of hurricane behavior under polluted oceanic conditions

It is worth noting that our modeling study assumes no time-varying sources of aerosols during the model integration, which may introduce uncertainty to the simulated aerosol budget. In addition, the microphysical scheme used in our model does not link ice heterogeneous nucleation with the prognostic aerosols as ice-nucleating particles, and ice nucleating particles have been shown to be crucial for ice phase cloud simulations in the convective storms (Jin et al., 2014; Zhao et al., 2019). Future improvements in the representations of the anthropogenic aerosols and their interactions with clouds in cloud-resolving models are necessary to advance the understanding of the aerosol-TC system with explicit representation of the air-sea interaction.

Code Availability

The code of WRF model used in this study is available at https://www2.mmm.ucar.edu/wrf/users/download/get_source.html (Skamarock and Klemp, 2008). Instructions for acquiring the code of ROMS can be found at https://www.myroms.org/ (Shchepetkin and McWilliams, 2005). The description of the coupling of WRF and ROMS is found in Patricola et al. (2012).

Data Availability

The hurricane Best Track Data is obtained from the tropical cyclone report by National Hurricane Center (https://www.nhc.noaa.gov/data/tcr/AL122005_Katrina.pdf, Knabb et al., 2023). The observed sea level height data at tide stations of Dauphin Island, New Canal and Shell Beach is available at https://tidesandcurrents.noaa.gov/stations.html?type=Water+Levels (NOAA, 2023).

All the WRF model simulation output used for this research can be downloaded from the website at http://web.gps.caltech.edu/~yzw/share/LinY-2023-ACP (Wang, 2023).

Author Contributions

Y.W. and R.Z. conceived and designed the research. Y.L., J.H., and Y.W. designed and performed the model simulation. All authors contributed to the model and observational data analyses and manuscript revision. Y.L., and Y.W. wrote the manuscript.

Acknowledgments

Y. Wang was supported by the NSF grant (award no. AGS-2103714). Additional support was provided by the Welch A. Foundation (A-1417). Y. Lin was supported by the NSF grant (award no., AGS-2103820) and NASA CCST (award no., 80NSSC23K0119) grant. J.H. Jiang acknowledged the support of the Jet Propulsion Laboratory, California Institute of Technology, under contract with NASA. Additional support was provided by the Welch A. Foundation (A-1417). We also acknowledge the computational support from Texas A&M High Performance Research Computing (HPRC) facility. All requests for materials in this paper should be addressed to Yuan Wang (yzwang@stanford.edu).

Competing interests

At least one of the (co-)authors is a member of the editorial board of Atmospheric Chemistry and Physics. The peer-review process was guided by an independent editor, and the authors also have no other competing interests to declare

References

Bates, T. S., Quinn, P. K., Coffman, D., Schulz, K., Covert, D. S., Johnson, J. E., Williams, E. J., Lerner, B. M., Angevine, W. M., Tucker, S. C., Brewer, W. A., and Stohl, A.: Boundary layer aerosol chemistry during TexAQS/GoMACCS 2006: Insights into aerosol sources and transformation processes, J. Geophys. Res., 113, n/a-n/a, 10.1029/2008JD010023, 2008.

Bender, M. A. and Ginis, I.: Real-case simulations of hurricane-ocean interaction using a high-resolution coupled model: Effects on hurricane intensity, Mon. Weather Rev., 128, 917-946, Doi 10.1175/1520-0493(2000)128<0917:Rcsoho>2.0.Co;2, 2000.

Bender, M. A., Ginis, I., and Kurihara, Y.: Numerical simulations of tropical cyclone-ocean interaction with a high-resolution coupled model, J. Geophys. Res., 98, 23245-23263, 10.1029/93JD02370, 1993.

Binkowski, F. S. and Roselle, S. J.: Models ‐ 3 Community Multiscale Air Quality (CMAQ) model aerosol component 1. Model description, J. Geophys. Res., 108, doi:10.1029/2001JD001409, 2003.

Black, P. G., D'Asaro, E. A., Sanford, T. B., Drennan, W. M., Zhang, J. A., French, J. R., Niiler, P. P., Terrill, E. J., and Walsh, E. J.: Air–sea exchange in hurricanes: synthesis of observations from the coupled boundary layer air–sea transfer experiment, Bull. Am. Meteorol. Soc., 88, 357-374, 10.1175/BAMS-88-3-357, 2007.

Chavas, D. R., Lin, N., Dong, W., and Lin, Y.: Observed tropical cyclone size revisited, J. Clim., 29, 2923-2939, 10.1175/jcli-d-15-0731.1, 2016.

Emanuel, K.: Increasing destructiveness of tropical cyclones over the past 30 years, Nature, 436, 686-688, 10.1038/nature03906, 2005.

Emanuel, K.: Assessing the present and future probability of Hurricane Harvey's rainfall, Proc. Nat. Acad. Sci. U.S.A., 114, 12681-12684, 10.1073/pnas.1716222114, 2017.

Emanuel, K. A.: An air-sea interaction theory for tropical cyclones. Part I: Steady-state maintenance, J. Atmos. Sci., 43, 585-605, 10.1175/1520-0469(1986)043<0585:aasitf>2.0.co;2, 1986.

Fan, J., Zhang, R. Y., Li, G. H., and Tao, W. K.: Effects of aerosols and relative humidity on cumulus clouds, J. Geophys. Res., 112, D14204, 10.1029/2006jd008136, 2007a.

Fan, J., Zhang, R., Li, G., Tao, W.-K., and Li, X.: Simulations of cumulus clouds using a spectral microphysics cloud-resolving model, J. Geophys. Res., 112, D04201, 10.1029/2006jd007688, 2007b.

Fan, J., Zhang, R. Y., Li, G. H., Nielsen-Gammon, J., and Li, Z. Q.: Simulations of fine particulate matter (PM2.5) in Houston, Texas, J. Geophys. Res., 110, D16203, 10.1029/2005jd005805, 2005.

Fan, J. W., Zhang, R. Y., Collins, D., and Li, G. H.: Contribution of secondary condensable organics to new particle formation: A case study in Houston, Texas, Geophys. Res. Lett., 33, Artn L15802, 10.1029/2006gl026295, 2006.

Fan, J. W., Rosenfeld, D., Zhang, Y. W., Giangrande, S. E., Li, Z. Q., Machado, L. A. T., Martin, S. T., Yang, Y., Wang, J., Artaxo, P., Barbosa, H. M. J., Braga, R. C., Comstock, J. M., Feng, Z., Gao, W. H., Gomes, H. B., Mei, F., Pohlker, C., Pohlker, M. L., Poschl, U., and de Souza, R. A. F.: Substantial convection and precipitation enhancements by ultrafine aerosol particles, Science, 359, 411-418, 10.1126/science.aan8461, 2018.

Fritz, H. M., Blount, C., Sokoloski, R., Singleton, J., Fuggle, A., McAdoo, B. G., Moore, A., Grass, C., and Tate, B.: Hurricane Katrina storm surge distribution and field observations on the Mississippi Barrier Islands, Estuar. Coast. Shelf Sci., 74, 12-20, 10.1016/j.ecss.2007.03.015, 2007.

Fritz, H. M., Blount, C., Sokoloski, R., Singleton, J., Fuggle, A., McAdoo, B. G., Moore, A., Grass, C., and Tate, B.: Hurricane Katrina storm surge reconnaissance, J. Geotech. Geoenviron., 134, 644-656, 10.1061/(Asce)1090-0241(2008)134:5(644), 2008.

Green, B. W. and Zhang, F.: Impacts of air–sea flux parameterizations on the intensity and structure of tropical cyclones, Mon. Weather Rev., 141, 2308-2324, 10.1175/MWR-D-12-00274.1, 2013.

Herbener, S. R., Heever, S. C. v. d., Carrió, G. G., Saleeby, S. M., and Cotton, W. R.: Aerosol indirect effects on idealized tropical cyclone dynamics, J. Atmos. Sci., 71, 2040-2055, 10.1175/jas-d-13-0202.1, 2014.

Houze, R. A., Chen, S. S., Smull, B. F., Lee, W.-C., and Bell, M. M.: Hurricane intensity and eyewall replacement, Science, 315, 1235-1239, 10.1126/science.1135650, 2007.

Jin, Y., Wang, S. P., Nachamkin, J., Doyle, J. D., Thompson, G., Grasso, L., Holt, T., Moskaitis, J., Jin, H., Hodur, R. M., Zhao, Q. Y., Liu, M., and DeMaria, M.: The Impact of Ice Phase Cloud Parameterizations on Tropical Cyclone Prediction, Mon. Weather Rev., 142, 606-625, 10.1175/Mwr-D-13-00058.1, 2014.

Knabb, D., Rhome, J.R., and Brown, D.P.: Tropical Cyclone Report Hurricane Katrina 23-30 August 2005, National Hurricane Center, https://www.nhc.noaa.gov/data/tcr/AL122005_Katrina.pdf (last access: 16 August 2023), 2023.

Khain, A., Lynn, B., and Dudhia, J.: Aerosol effects on intensity of landfalling hurricanes as seen from simulations with the WRF model with spectral bin microphysics, J. Atmos. Sci., 67, 365-384, doi:10.1175/2009JAS3210.1, 2010.

Khain, A., Lynn, B., and Shpund, J.: High resolution WRF simulations of Hurricane Irene: Sensitivity to aerosols and choice of microphysical schemes, Atmos. Res., 167, 129-145, http://dx.doi.org/10.1016/j.atmosres.2015.07.014, 2016.

Khain, A., Cohen, N., Lynn, B., and Pokrovsky, A.: Possible aerosol effects on lightning activity and structure of hurricanes, J. Atmos. Sci., 65, 3652-3677, 10.1175/2008JAS2678.1, 2008.

Khain, A. P. and Ginis, I.: The mutual response of a moving tropical cyclone and the ocean, Beitr. Phys. Atmos., 64, 125-141, 1991.

Khain, A., Lynn, B., and Dudhia, J.: Aerosol effects on intensity of landfalling hurricanes as seen from simulations with the WRF model with spectral bin microphysics, J. Atmos. Sci., 67, 365-384, doi:10.1175/2009JAS3210.1, 2010.

Knutson, T., Camargo, S. J., Chan, J. C. L., Emanuel, K., Ho, C. H., Kossin, J., Mohapatra, M., Satoh, M., Sugi, M., Walsh, K., and Wu, L. G.: Tropical cyclones and climate change assessment: Part I: detection and attribution, Bull. Am. Meteorol. Soc., 100, 1987-2007, 10.1175/Bams-D-18-0189.1, 2019.

Levy, M. E., Zhang, R. Y., Khalizov, A. F., Zheng, J., Collins, D. R., Glen, C. R., Wang, Y., Yu, X. Y., Luke, W., Jayne, J. T., and Olaguer, E.: Measurements of submicron aerosols in Houston, Texas during the 2009 SHARP field campaign, J. Geophys. Res., 118, 10518-10534, 10.1002/Jgrd.50785, 2013.

Levy, R. C., Leptoukh, G. G., Kahn, R., Zubko, V., Gopalan, A., and Remer, L. A.: A critical look at deriving monthly aerosol optical depth from satellite data, IEEE Trans. Geosci. Remote Sens., 47, 2942-2956, Doi 10.1109/Tgrs.2009.2013842, 2009.

Li, G., Wang, Y., and Zhang, R.: Implementation of a two-moment bulk microphysics scheme to the WRF model to investigate aerosol-cloud interaction, J. Geophys. Res., 113, D15211, 10.1029/2007jd009361, 2008.

Li, G., Wang, Y., Lee, K.-H., Diao, Y., and Zhang, R.: Impacts of aerosols on the development and precipitation of a mesoscale squall line, J. Geophys. Res., 114, D17205, 10.1029/2008jd011581, 2009.

Lin, Y., Zhao, M., and Zhang, M.: Tropical cyclone rainfall area controlled by relative sea surface temperature, Nature Communications, 6, 6591, 10.1038/ncomms7591, 2015.

Lin, Y., Wang, Y., Pan, B., Hu, J., Liu, Y., and Zhang, R.: Distinct Impacts of Aerosols on an Evolving Continental Cloud Complex during the RACORO Field Campaign, J. Atmos. Sci., 73, 3681-3700, 10.1175/jas-d-15-0361.1, 2016.

Liu, W. T., Katsaros, K. B., and Businger, J. A.: Bulk parameterization of air-sea exchanges of heat and water vapor including the molecular constraints at the interface, J. Atmos. Sci., 36, 1722-1735, 10.1175/1520-0469(1979)036<1722:bpoase>2.0.co;2, 1979.

Lynn, B. H., Khain, A. P., Bao, J. W., Michelson, S. A., Yuan, T., Kelman, G., Rosenfeld, D., Shpund, J., and Benmoshe, N.: The sensitivity of hurricane Irene to aerosols and ocean coupling: simulations with WRF spectral bin microphysics, J. Atmos. Sci., 73, 467-486, 10.1175/jas-d-14-0150.1, 2016.

Ma, Z., Fei, J., Liu, L., Huang, X., and Cheng, X.: Effects of the cold core eddy on tropical cyclone intensity and structure under idealized air–sea interaction conditions, Mon. Weather Rev., 141, 1285-1303, 10.1175/mwr-d-12-00123.1, 2013.

Montgomery, M. T. and Kallenbach, R. J.: A theory for vortex Rossby-waves and its application to spiral bands and intensity changes in hurricanes, Q. J. Roy. Meteorol. Soc., 123, 435-465, DOI 10.1002/qj.49712353810, 1997.

NOAA (National Oceanic and Atmospheric Administration): Water level data, NOAA Tides and Currents [data set], https://tidesandcurrents.noaa.gov/stations.html?type=Water+Levels (last access: 7 July 2023), 2023.

NWS (National Weather Service): A theory for vortex rossby-waves and its application to spiral bands and intensity changes in hurricanes, https://www.weather.gov/mob/katrina, 2016.

Orville, R. E., Huffines, G., Nielsen-Gammon, J., Zhang, R. Y., Ely, B., Steiger, S., Phillips, S., Allen, S., and Read, W.: Enhancement of cloud-to-ground lightning over Houston, Texas, Geophys. Res. Lett., 28, 2597-2600, Doi 10.1029/2001gl012990, 2001.

Pan, B., Wang, Y., Hu, J., Lin, Y., Hsieh, J.-S., Logan, T., Feng, X., Jiang, J. H., Yung, Y. L., and Zhang, R.: Impacts of Saharan dust on Atlantic regional climate and implications for tropical cyclones, J. Clim., 31, 7621-7644, 10.1175/jcli-d-16-0776.1, 2018.

Pan, B. W., Wang, Y., Logan, T., Hsieh, J. S., Jiang, J. H., Li, Y. X., and Zhang, R. Y.: Determinant role of aerosols from industrial sources in hurricane Harvey's catastrophe, Geophys. Res. Lett., 47, ARTN e2020GL090014, 10.1029/2020GL090014, 2020.

Patricola, C. M., Chang, P., Li, M., Saravanan, R., Xu, Z., and Hsieh, J.-S.: An investigation of tropical Atlantic bias in a high-resolution coupled regional climate model, Climate Dynamic, 10.1007/s00382-012-1320-5, 2012.

Richard, D., Rhome, R., and Brown, P.: Hurricane Katrina (PDF) (Report). Tropical Cyclone Report. National Hurricane Center, https://www.nhc.noaa.gov/data/tcr/AL122005_Katrina.pdf, December 20, 2005 (accessed on April 23, 2023).

Rosenfeld, D., Clavner, M., and Nirel, R.: Pollution and dust aerosols modulating tropical cyclones intensities, Atmos. Res., 102, 66-76, 10.1016/j.atmosres.2011.06.006, 2011.

Rosenfeld, D., Woodley, W. L., Khain, A., Cotton, W. R., Carrió, G., Ginis, I., and Golden, J. H.: Aerosol effects on microstructure and intensity of tropical cyclones, Bull. Am. Meteorol. Soc., 10.1175/BAMS-D-11-00147.1, 2012.

Saha, S., Moorthi, S., Pan, H.-L., Wu, X., Wang, J., Nadiga, S., Tripp, P., Kistler, R., Woollen, J., Behringer, D., Liu, H., Stokes, D., Grumbine, R., Gayno, G., Wang, J., Hou, Y.-T., Chuang, H.-y., Juang, H.-M. H., Sela, J., Iredell, M., Treadon, R., Kleist, D., Delst, P. V., Keyser, D., Derber, J., Ek, M., Meng, J., Wei, H., Yang, R., Lord, S., Dool, H. v. d., Kumar, A., Wang, W., Long, C., Chelliah, M., Xue, Y., Huang, B., Schemm, J.-K., Ebisuzaki, W., Lin, R., Xie, P., Chen, M., Zhou, S., Higgins, W., Zou, C.-Z., Liu, Q., Chen, Y., Han, Y., Cucurull, L., Reynolds, R. W., Rutledge, G., and Goldberg, M.: The NCEP climate forecast system reanalysis, Bull. Am. Meteorol. Soc., 91, 1015-1058, 10.1175/2010bams3001.1, 2010.

Schade, L. R. and Emanuel, K. A.: The ocean's effect on the intensity of tropical cyclones: Results from a simple coupled atmosphere–ocean model, J. Atmos. Sci., 56, 642-651, 10.1175/1520-0469(1999)056<0642:toseot>2.0.co;2, 1999.

Shchepetkin, A. F. and McWilliams, J. C.: The regional oceanic modeling system (ROMS): a split-explicit, free-surface, topography-following-coordinate oceanic model, Ocean Modelling, 9, 347-404, https://doi.org/10.1016/j.ocemod.2004.08.002, 2005.

Shpund, J., Khain, A., and Rosenfeld, D.: Effects of Sea Spray on Microphysics and Intensity of Deep Convective Clouds Under Strong Winds, J. Geophys. Res., 124, 9484-9509, 10.1029/2018jd029893, 2019.

Shi, J. J., Braun, S. A., Tao, Z., and Matsui, T.: Influence of the Saharan Air Layer on Hurricane Nadine (2012). Part I: Observations from the Hurricane and Severe Storm Sentinel (HS3) Investigation and Modeling Results, Mon. Weather Rev., 149, 3541-3562, https://doi.org/10.1175/MWR-D-20-0344.1, 2021.

Skamarock, W. C. and Klemp, J. B.: A time-split nonhydrostatic atmospheric model for weather research and forecasting applications, J Comput Phys, 227, 3465-3485, https://doi.org/10.1016/j.jcp.2007.01.037, 2008.

Souri, A. H., Choi, Y., Kodros, J. K., Jung, J., Shpund, J., Pierce, J. R., Lynn, B. H., Khain, A., and Chance, K.: Response of Hurricane Harvey's rainfall to anthropogenic aerosols: A sensitivity study based on spectral bin microphysics with simulated aerosols, Atmos. Res., 242, 104965, https://doi.org/10.1016/j.atmosres.2020.104965, 2020.

Sun, Y. and Zhao, C.: Influence of Saharan Dust on the Large-Scale Meteorological Environment for Development of Tropical Cyclone Over North Atlantic Ocean Basin, J. Geophys. Res., 125, e2020JD033454, https://doi.org/10.1029/2020JD033454, 2020.

Trenberth, K. E., Cheng, L. J., Jacobs, P., Zhang, Y. X., and Fasullo, J.: Hurricane Harvey links to ocean heat content and climate change adaptation, Earths Future, 6, 730-744, 10.1029/2018ef000825, 2018.

van Oldenborgh, G. J., van der Wiel, K., Sebastian, A., Singh, R., Arrighi, J., Otto, F., Haustein, K., Li, S. H., Vecchi, G., and Cullen, H.: Attribution of extreme rainfall from Hurricane Harvey, August 2017, Environ. Res. Lett., 12, ARTN 124009, 10.1088/1748-9326/aa9ef2, 2017.

Wang, Y., Lee, K.-H., Lin, Y., Levy, M., and Zhang, R.: Distinct effects of anthropogenic aerosols on tropical cyclones, Nature Climate Change, 4, 368-373, 10.1038/nclimate2144, 2014.

Wang, Y., Wan, Q., Meng, W., Liao, F., Tan, H., and Zhang, R.: Long-term impacts of aerosols on precipitation and lightning over the Pearl River Delta megacity area in China, Atmos. Chem. Phys., 11, 12421-12436, 10.5194/acp-11-12421-2011, 2011.

Wang, Y., Vogel, J. M., Lin, Y., Pan, B., Hu, J., Liu, Y., Dong, X., Jiang, J. H., Yung, Y. L., and Zhang, R.: Aerosol microphysical and radiative effects on continental cloud ensembles, Adv. Atmos. Sci., 35, 234-247, 10.1007/s00376-017-7091-5, 2018.

Wang, Y.: WRF-ROMS model output, Caltech Server [dataset], http://web.gps.caltech.edu/~yzw/share/LinY-2023-ACP (last access: 18 August 2023), 2023.

Wang, Y. Q.: Vortex Rossby waves in a numerically simulated tropical cyclone. Part II: The role in tropical cyclone structure and intensity changes, J. Atmos. Sci., 59, 1239-1262, Doi 10.1175/1520-0469(2002)059<1239:Vrwian>2.0.Co;2, 2002.

Woodruff, J. D., Irish, J. L., and Camargo, S. J.: Coastal flooding by tropical cyclones and sea-level rise, Nature, 504, 44-52, 10.1038/nature12855, 2013.

Yablonsky, R. M. and Ginis, I.: Limitation of one-dimensional ocean models for coupled hurricane–ocean model forecasts, Mon. Weather Rev., 137, 4410-4419, 10.1175/2009mwr2863.1, 2009.

Zhang, H., McFarquhar, G. M., Cotton, W. R., and Deng, Y.: Direct and indirect impacts of Saharan dust acting as cloud condensation nuclei on tropical cyclone eyewall development, Geophys. Res. Lett., 36, n/a-n/a, 10.1029/2009GL037276, 2009.

Zhang, K. M., Knipping, E. M., Wexler, A. S., Bhave, P. V., and Tonnesen, G. S.: Size distribution of sea-salt emissions as a function of relative humidity, Atmos. Environ., 39, 3373-3379, https://doi.org/10.1016/j.atmosenv.2005.02.032, 2005.

Zhang, R., Wang, G., Guo, S., Zamora, M. L., Ying, Q., Lin, Y., Wang, W., Hu, M., and Wang, Y.: Formation of urban fine particulate matter, Chemical Reviews, 115, 3803-3855, 10.1021/acs.chemrev.5b00067, 2015.

Zhang, W., Villarini, G., Vecchi, G. A., and Smith, J. A.: Urbanization exacerbated the rainfall and flooding caused by hurricane Harvey in Houston, Nature, 563, 384-+, 10.1038/s41586-018-0676-z, 2018.

Zhao, B., Wang, Y., Gu, Y., Liou, K. N., Jiang, J. H., Fan, J., Liu, X., Huang, L., and Yung, Y. L.: Ice nucleation by aerosols from anthropogenic pollution, 10.1038/s41561-019-0389-4, 2019.

Zhao, C. F., Lin, Y. L., Wu, F., Wang, Y., Li, Z. Q., Rosenfeld, D., and Wang, Y.: Enlarging rainfall area of tropical cyclones by atmospheric aerosols, Geophys. Res. Lett., 45, 8604-8611, 10.1029/2018gl079427, 2018.

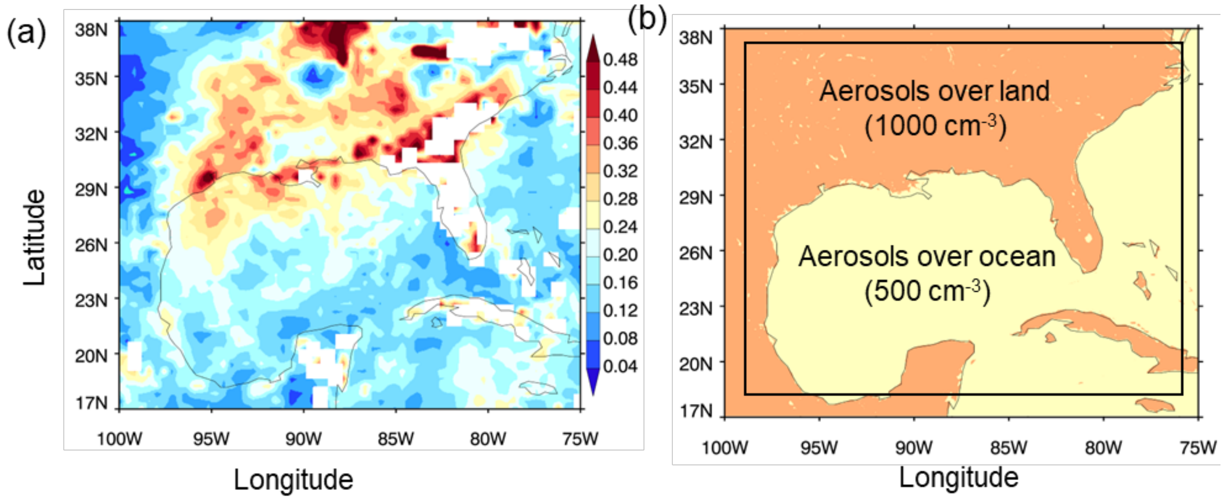

Figure 1. (a) MODIS AOD distribution averaged over the period prior to and during Hurricane Katrina 2005 passage over the Gulf of Mexico (Aug. 24 – Aug. 31). (b) The initial condition of aerosol concentrations with land-ocean contrast for the polluted case in CR-WRF. The black square in (b) denotes the domain for the ROMS model.

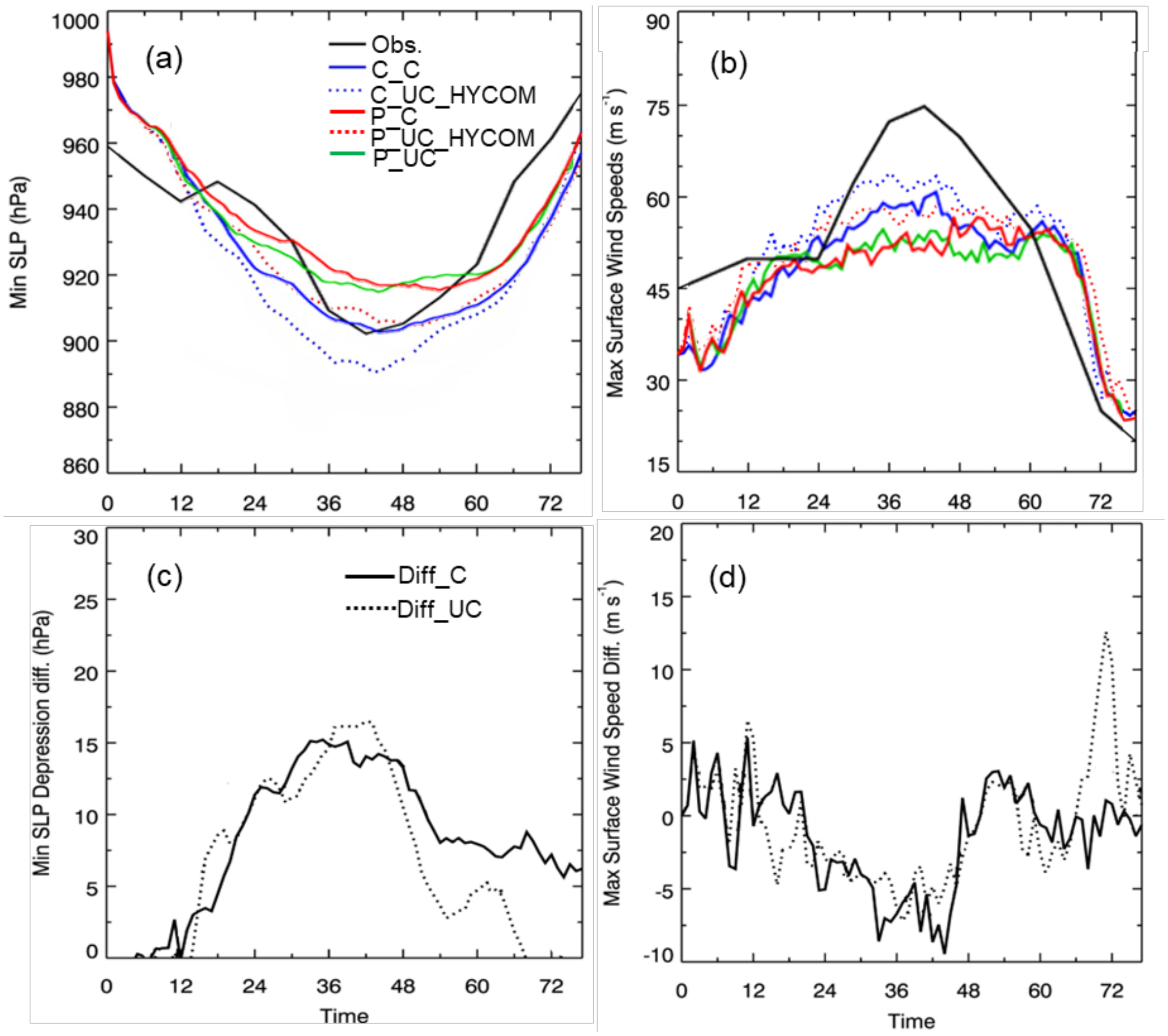

Figure 2. The simulated and observed evolution of the hurricane in terms of (a) minimum sea-level pressure (SLP) and (b) maximum surface (10-m) wind speed for the coupled and uncoupled simulations, i.e., C_C (blue solid lines) and P_C (red solid lines), C_UC_HYCOM (blue dotted lines) and P_UC_HYCOM (red dotted lines), as well the P_UC case (solid green line). The differences of minimum SLP (c) and maximum surface (10-m) wind speed (d) between clean and polluted simulation are shown for the coupled (Diff_C = P_C – C_C, solid lines) and uncoupled cases (Diff_UC = P_UC_HYCOM – C_UC_HYCOM, dotted lines). The observations (black) in (a) and (b) are from the NHC Best Track Data.

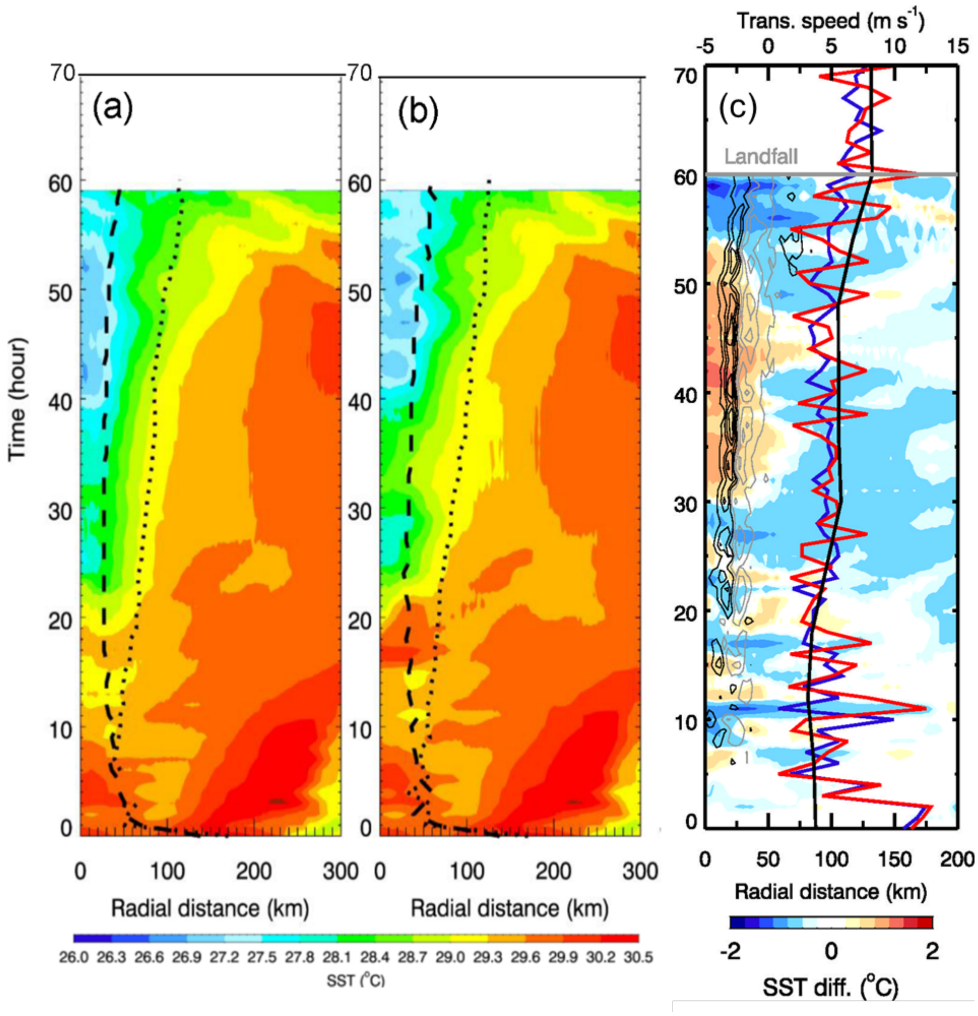

785

786 **Figure 3**. Hovmöller diagrams of azimuthal mean SST fields for (a) C_C and (b) P_C, as well as

787 their differences (P_C - C_C). The solid and dash lines throughout the entire hurricane lifecycles

788 in panels (a-c) denote the RMW and the radii for the hurricane force wind (>34 m s-1),

789 respectively. Contour lines in panel (c) denote the changes in surface wind stress curl (with an

790 interval of 0.25 N m^{-2} and grey for positive and black for negative changes). The curves denote

791 the hurricane translation speeds for observation (black), C_C (blue), and P_C (red).

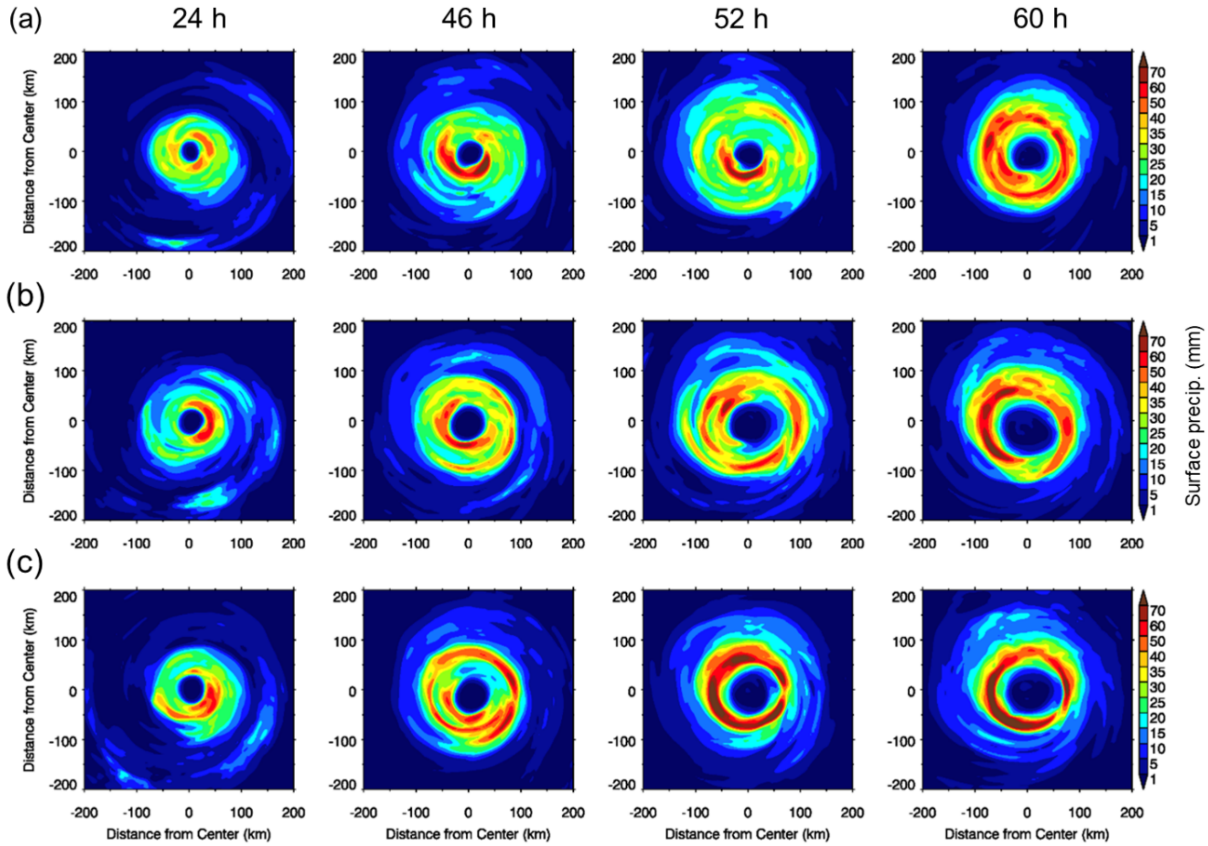

Figure 4. Horizontal distribution of precipitation rates for (a) C_C, (b) P_UC, and (c) P_C. Snapshots at four times are displayed, including 24, 46, 52, and 60 h from the start of simulations, corresponding to the developing stage, two mature stages, and dissipating stage of TC, respectively.

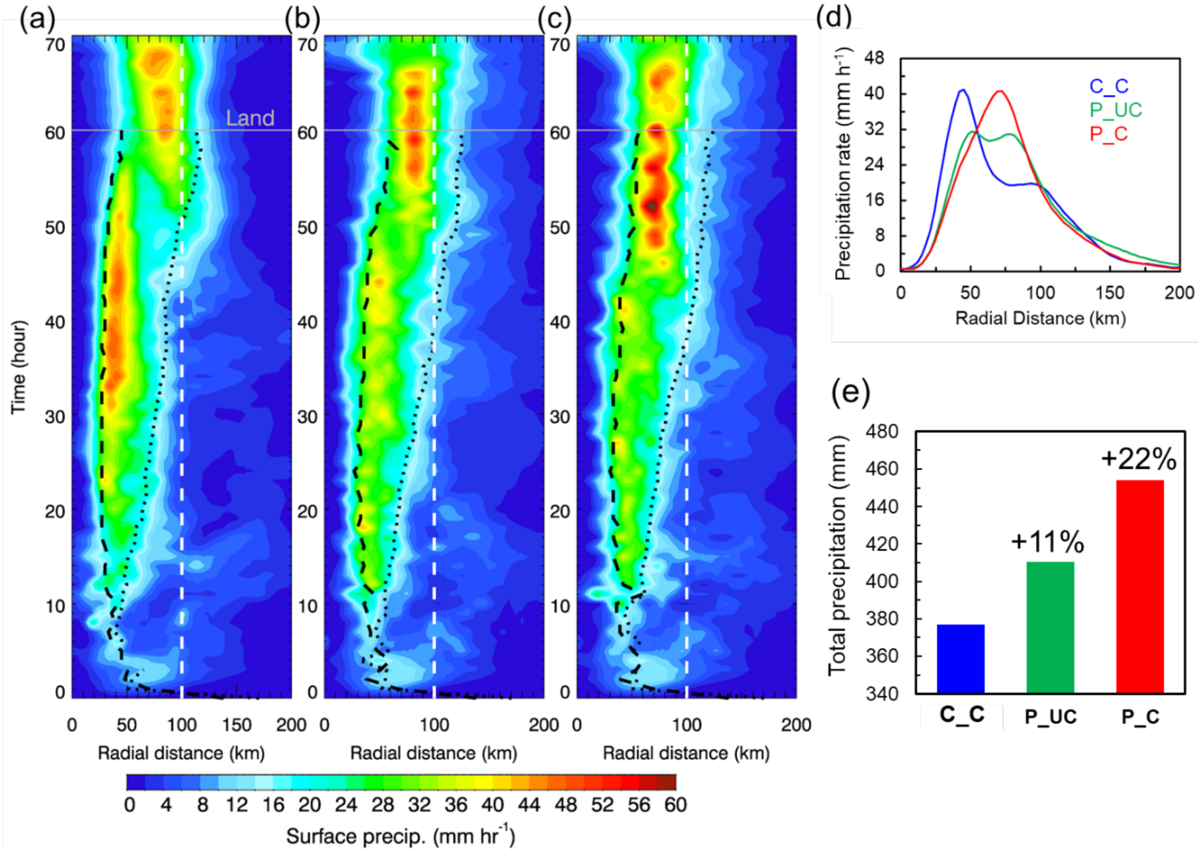

Figure 5. Hovmöller diagrams of the azimuthal means changes of precipitation rate for (a) C_C, (b) P_UC, and (c) P_C. The white dash lines in (a-c) denote the distance of 100 km away from the storm center. The solid and dash black lines (a-c) represent the radii of the maximum wind speed (RMW) and the hurricane force wind (with wind speed >32 m s^{-1}), respectively. (d) Azimuthally-averaged radial profiles of precipitation rate and (e) total accumulated precipitation for C_C (blue), P_UC (green), and P_C (red) within 100 km of the storm center during the mature stage of TC, corresponding to the time period of 40-55 h from the beginning of TC simulations.

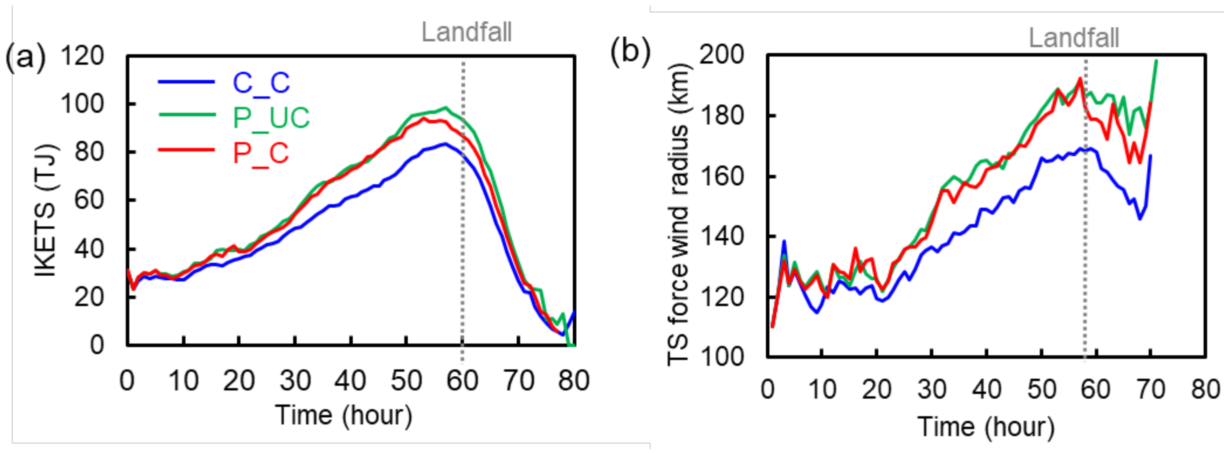

Figure 6. Temporal evolutions of (a) integrated kinetic energy (IKE) and (b) storm force radius with winds higher than tropical storm force, i.e., 18 m s^{-1}, for C_C (blue), P_UC (green), and P_C (red). The dot grey lines (a, b) denote the hurricane landfall time.

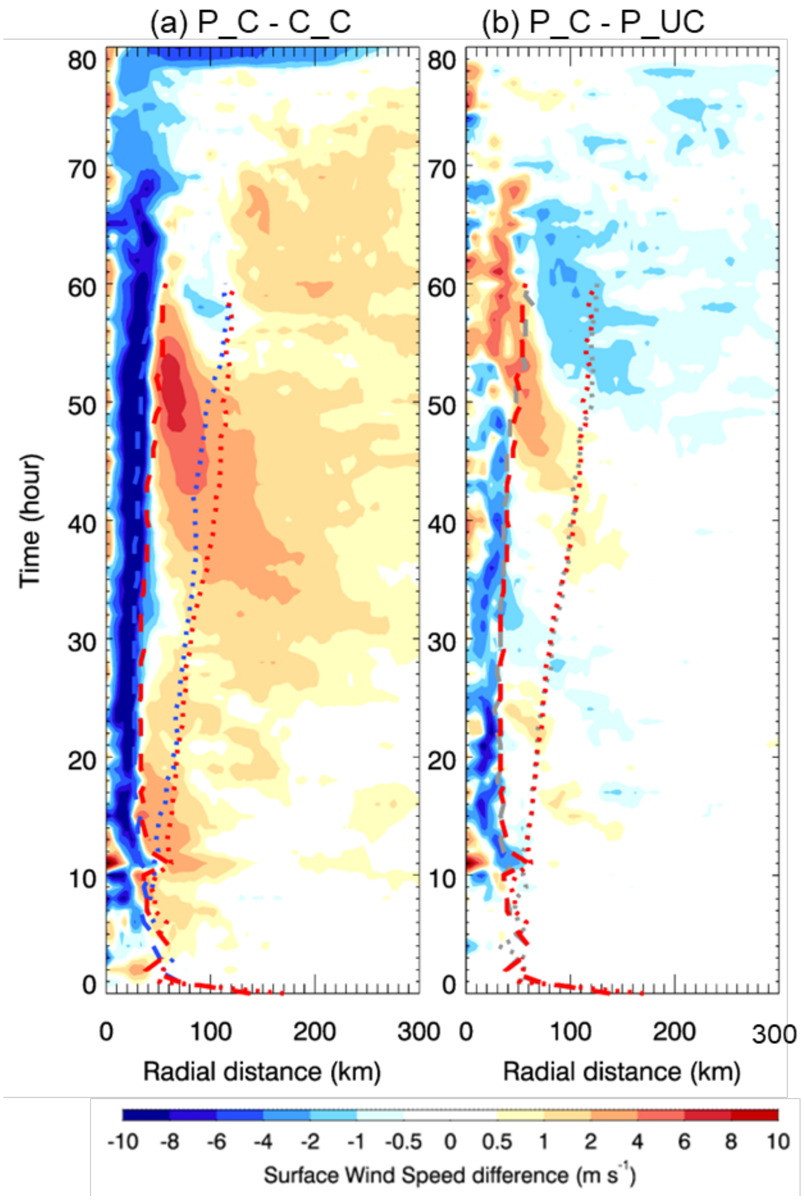

Figure 7. Hovmöller diagrams of the changes in azimuthal means of surface wind speed for (a) P_C – C_C and (b) P_C – P_UC. The dashed and dotted curves throughout the entire hurricane lifecycles denote the RMW and the radii for the hurricane force wind, respectively, with different colors (blue, green, and red) representing different cases (C_C, P_UC, and P_C).

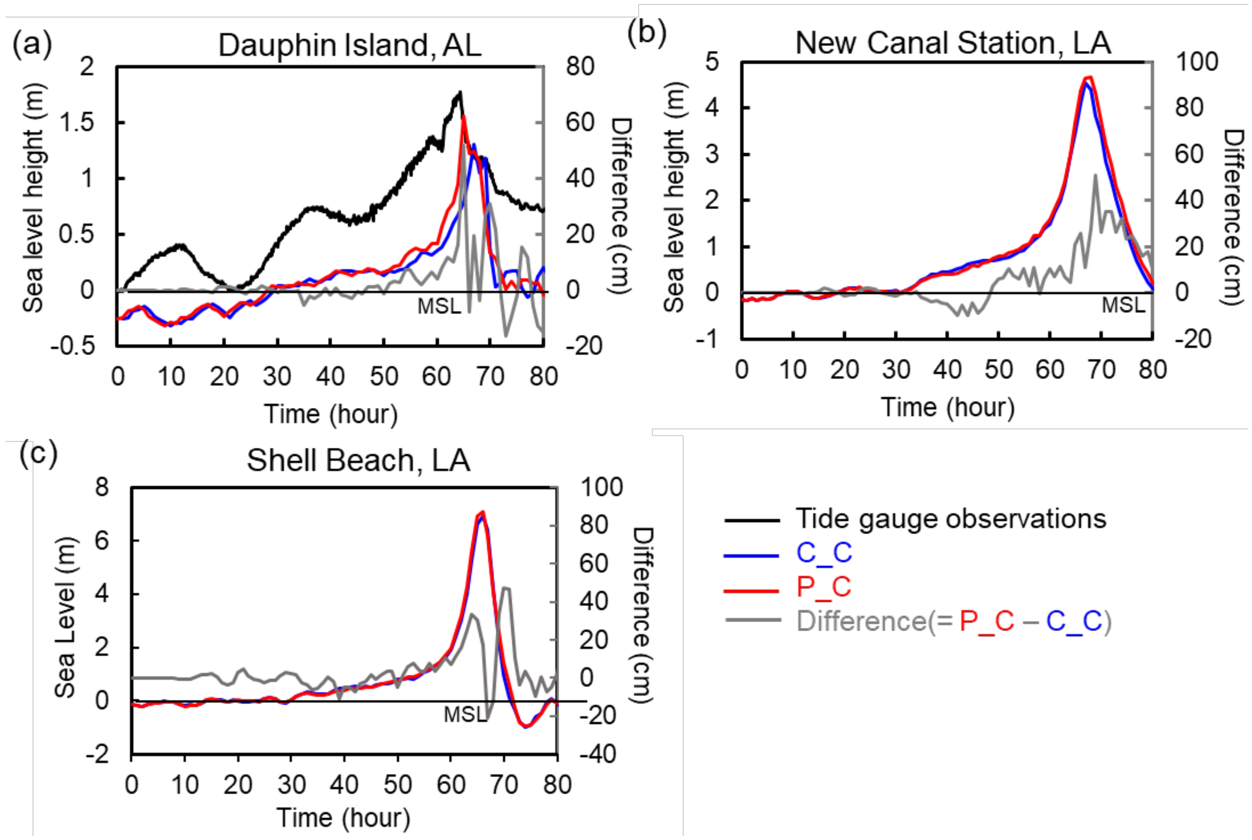

Figure 8. Sea level height at three coastal sites near New Orleans: (a) Dauphin Island, AL, (b) New Canal Station, LA, and (c) Pass Christian, MS for C_C (blue) and P_C (red) cases. The gauge observation (black line) is only available at Dauphin site in (a). The grey lines denote the differences between P_C and C_C cases.

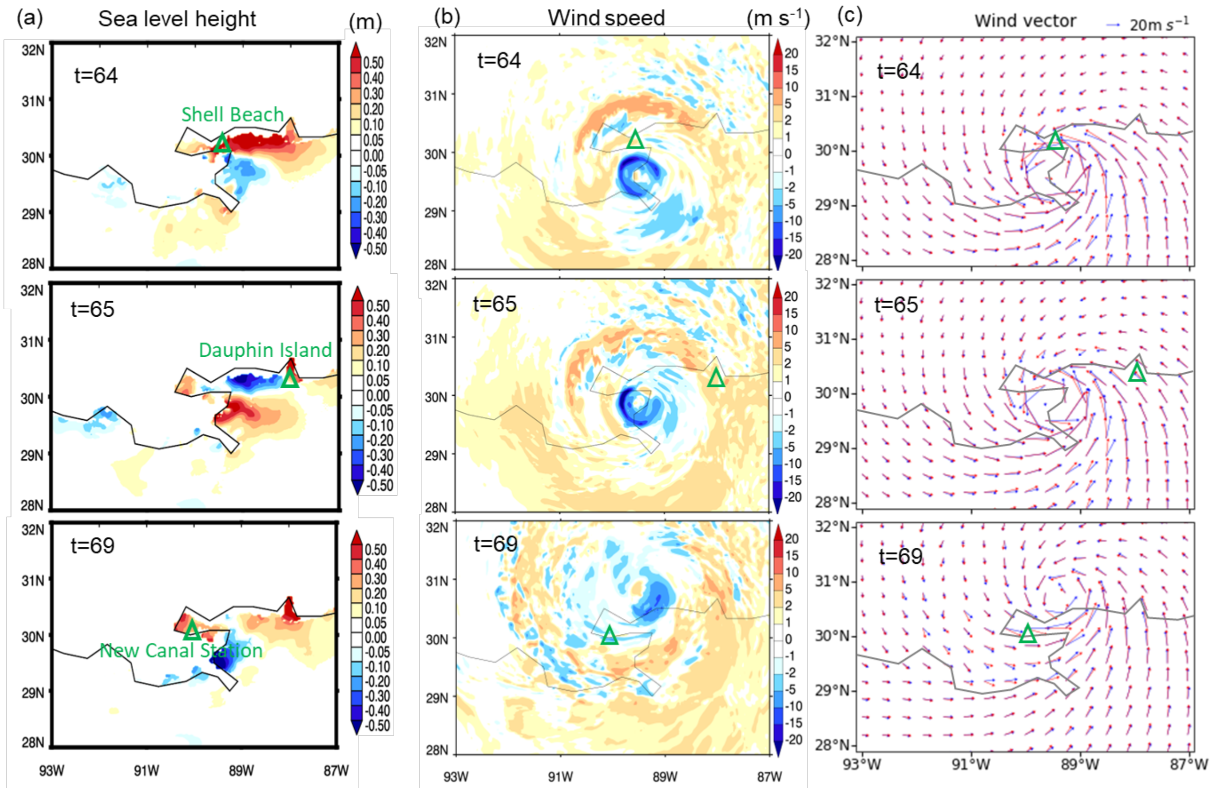

Figure 9. The differences in (a) sea level height and (b) wind speed between P_C – and C-C cases and (c) wind vectors for both C_C (blue) and P_C (red) cases over New Orleans coastal region at hour 64, 65, and 69 from simulation start when Hurricane Katrina made landfall. The green triangles in (a) denote the gauge station, including Shell Beach, AL, Dauphin Island, AL, and New Canal Station, LA.

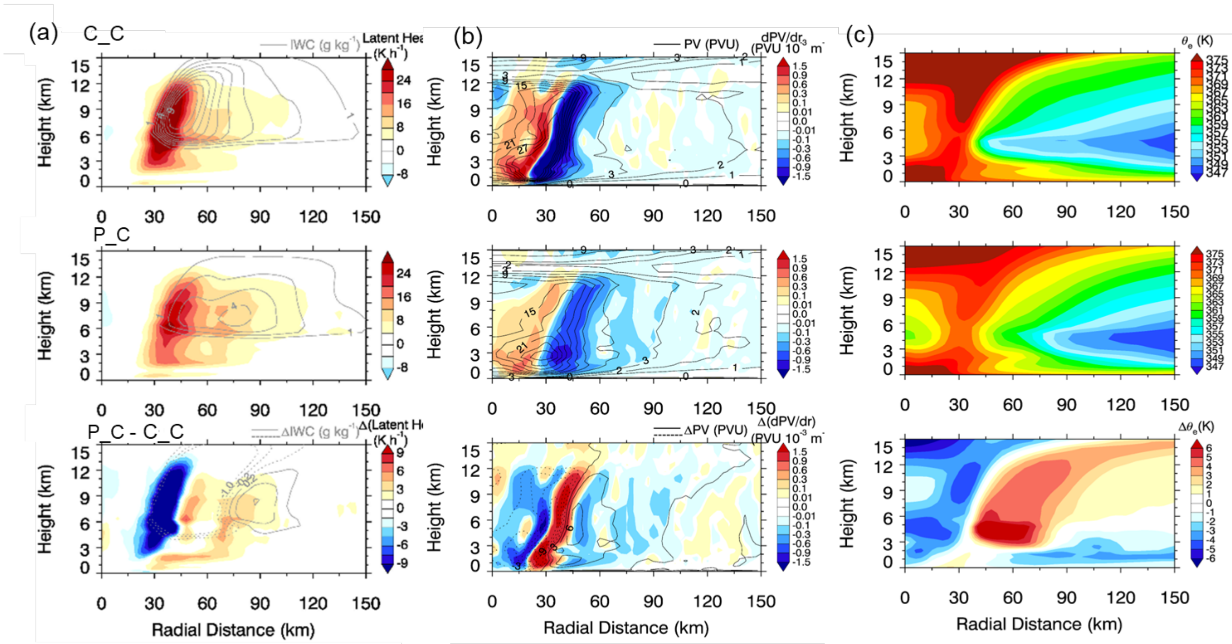

Figure 10. Vertical-radial cross-sections of 20-hr (32–52 hour) azimuthal means of (a) latent heat overlaid with ice water content (IWC), (b) equivalent potential temperature (θ_e), and (c) potential vorticity (PV) and its gradient for C_C, P_C case, and their difference (P_C - C_C) from top to bottom.

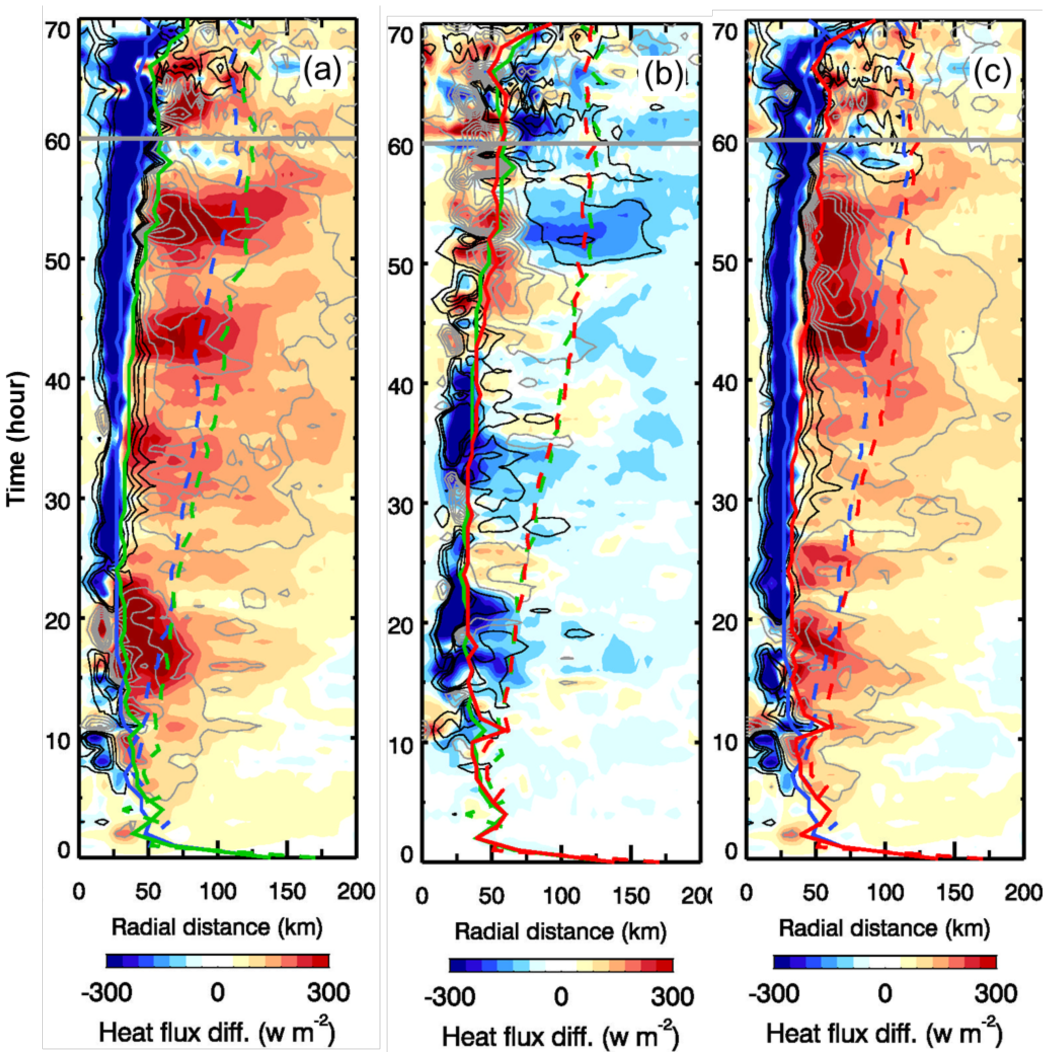

Figure 11. Hovmöller diagrams of the changes of azimuthal means in surface wind stress (contour lines, with an interval of 0.4 N m^{-2} and grey for positive and black for negative changes) and surface total heat flux (color shading) induced by (a) aerosol only effect (i.e., P_UC – C_C), (b) ocean coupling effect (i.e., P_C – P_UC), and (c) the combined effect (i.e., P_C – C_C). The solid and dashed curves throughout the entire hurricane lifecycles denote the RMW and the radii for the hurricane force wind (>34 m s^{-1}), respectively, with different colors (blue, green, and red) representing different cases (C_C, P_UC, and P_C). The positive (negative) perturbations denote the upward (downward) flux, i.e., from the ocean (the atmosphere) to the atmosphere (the ocean).

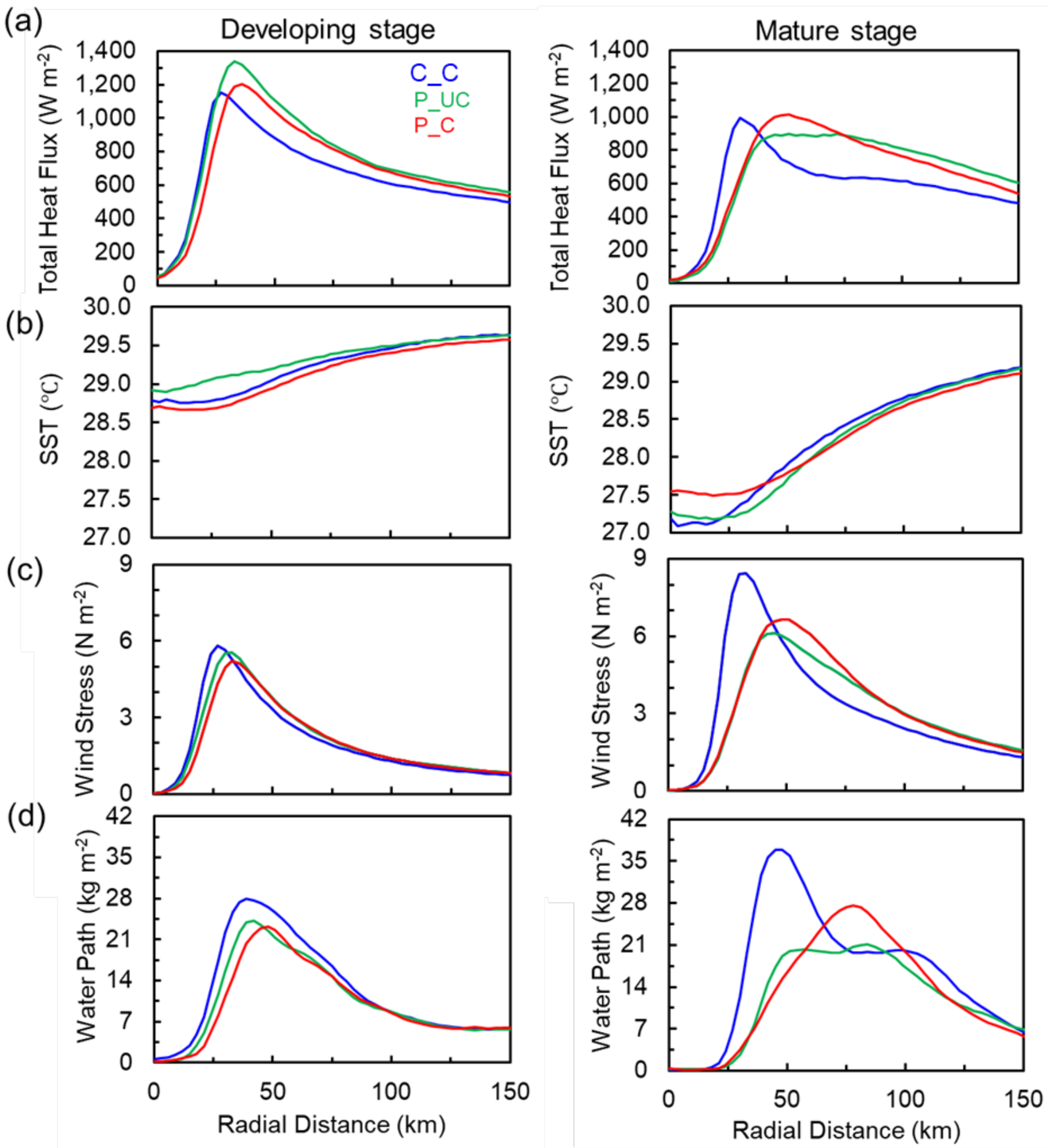

Figure 12. Azimuthally-averaged radial profiles for (a) total heat flux at the ocean surface, (b) SST, (c) wind stress, and (d) total condensate water path for C_C (blue), P_UC (green), and P_C (red) cases for the developing stage (15-28 h, left column) and mature stage (42-55 h, right column).

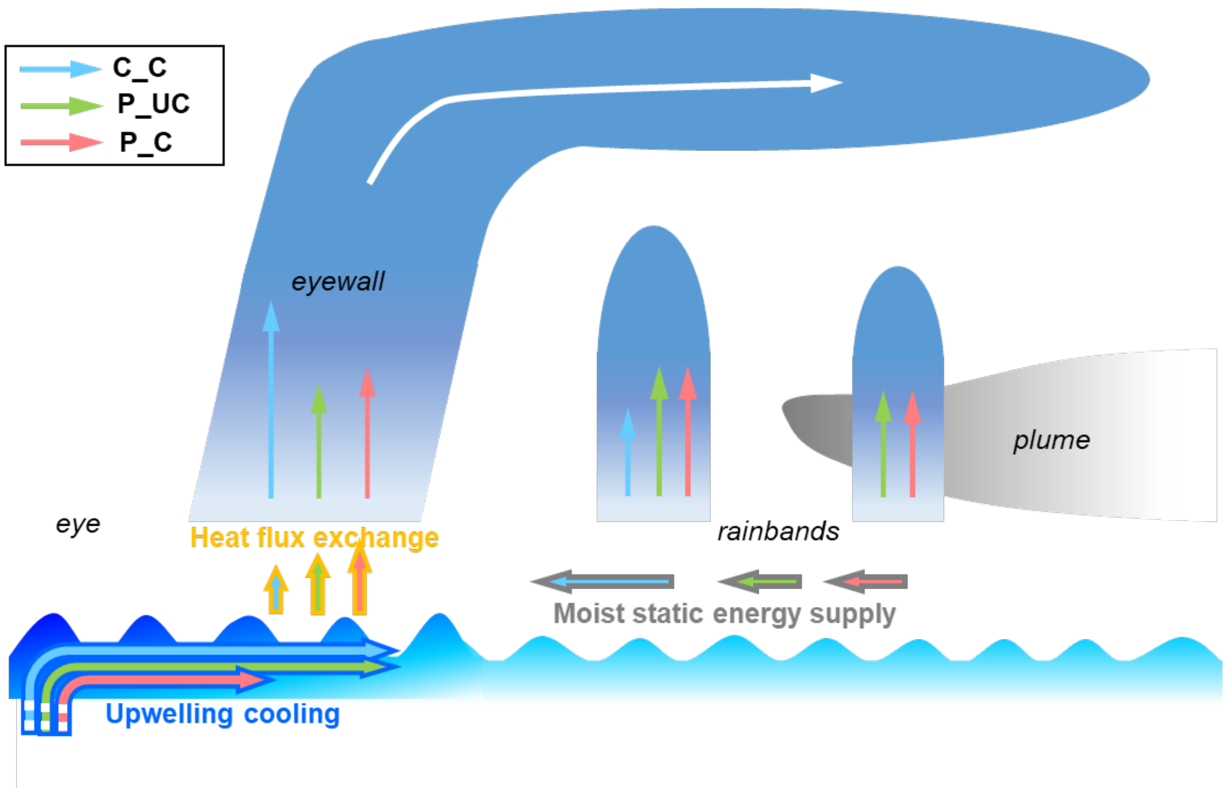

Figure 13. A schematic of the effects of anthropogenic aerosols and ocean feedback on a hurricane. The development of hurricane is characterized by convection in the outer rainbands and eyewall (vertical arrows). The moist static energy supply in the lower-level inflow (grey-edged horizontal arrows pointing from outer rainbands to storm core), the vertical mixing cooling in the ocean beneath the storm (blue-edged arrows starting in deep ocean and pointing from storm core to outer rainbands), and the heat flux exchange between the ocean and the storm (orange-edged vertical arrows pointing from the ocean to the storm near the storm core) are depicted in different types of arrows. The aerosol microphysical effect in the uncoupled polluted case (P_UC, green arrows) enhances convection in outer rainbands by invigorating mixed-phase cloud processes, leading to drier and colder lower-level inflow to the storm core and a weakened eyewall. Comparing the coupled polluted case (P_C, red arrows) to the coupled clean case (C_C, blue arrows), the weakening of the storm intensity by aerosols reduces the vertical mixing

cooling in the ocean because of the smaller surface wind stress. Consequently, the increased sea surface temperature further re-energizes storm circulation. Therefore, the ocean coupling mitigates the aerosol weakening effect to some extent. The overall effect of aerosol microphysical effects and ocean coupling results in moderate enhancement of convection in the eyewall, stronger than that in the clean case (blue arrows) but weaker than that in the uncoupled polluted case.

Table 1. Experiment list.

Cases	Aerosol configuration	Coupling	SST
C_C	The initial and boundary loadings of anthropogenic aerosols over land/ocean: 200/100 cm^{-3}; Sea salt: Initial concentration of 100 cm^{-3} with continuous emissions as a function of surface wind speed	Yes	IC/BC based on HYCOM; Updated by ROMS every 10 min
C_UC_HYCOM	As C_C	No	Constrained by HYCOM and fixed
P_C	As C_C, but with high loadings of anthropogenic aerosols over land/ocean of 1000/500 cm^{-3}	Yes	As C_C
P_UC	As P_C	No	Prescribed from outputs of C_C case
P_UC_HYCOM	As P_C	No	Constrained by HYCOM and fixed